The Astrophysical Journal, 721:975–994, 2010 October 1 doi:10.1088/0004-637X/721/2/975

REGULATION OF STAR FORMATION RATES IN MULTIPHASE GALACTIC DISKS: A THERMAL/DYNAMICAL EQUILIBRIUM MODEL

Eve C. Ostriker[1], Christopher F. McKee[2,3], and Adam K. Leroy[4,5]
[1] Department of Astronomy, University of Maryland, College Park, MD 20742, USA; ostriker@astro.umd.edu
[2] Departments of Physics and Astronomy, University of California, Berkeley, CA 94720, USA; cmckee@astro.berkeley.edu
[3] LERMA-LRA, Ecole Normale Superieure, 24 rue Lhomond, 75005 Paris, France
[4] National Radio Astronomy Observatory, 520 Edgemont Road, Charlottesville, VA 22903, USA; aleroy@nrao.edu
Received 2010 March 11; accepted 2010 July 30; published 2010 September 3

ABSTRACT

We develop a model for the regulation of galactic star formation rates $\Sigma_{\rm SFR}$ in disk galaxies, in which interstellar medium (ISM) heating by stellar UV plays a key role. By requiring that thermal and (vertical) dynamical equilibrium are simultaneously satisfied within the diffuse gas, and that stars form at a rate proportional to the mass of the self-gravitating component, we obtain a prediction for $\Sigma_{\rm SFR}$ as a function of the total gaseous surface density Σ and the midplane density of stars+dark matter $\rho_{\rm sd}$. The physical basis of this relationship is that the thermal pressure in the diffuse ISM, which is proportional to the UV heating rate and therefore to $\Sigma_{\rm SFR}$, must adjust until it matches the midplane pressure value set by the vertical gravitational field. Our model applies to regions where $\Sigma \lesssim 100\,M_\odot$ pc^{-2}. In low-$\Sigma_{\rm SFR}$ (outer-galaxy) regions where diffuse gas dominates, the theory predicts that $\Sigma_{\rm SFR} \propto \Sigma\sqrt{\rho_{\rm sd}}$. The decrease of thermal equilibrium pressure when $\Sigma_{\rm SFR}$ is low implies, consistent with observations, that star formation can extend (with declining efficiency) to large radii in galaxies, rather than having a sharp cutoff at a fixed value of Σ. The main parameters entering our model are the ratio of thermal pressure to total pressure in the diffuse ISM, the fraction of diffuse gas that is in the warm phase, and the star formation timescale in self-gravitating clouds; all of these are (at least in principle) direct observables. At low surface density, our model depends on the ratio of the mean midplane FUV intensity (or thermal pressure in the diffuse gas) to the star formation rate, which we set based on solar-neighborhood values. We compare our results to recent observations, showing good agreement overall for azimuthally averaged data in a set of spiral galaxies. For the large flocculent spiral galaxies NGC 7331 and NGC 5055, the correspondence between theory and observation is remarkably close.

Key words: galaxies: ISM – galaxies: spiral – ISM: kinematics and dynamics – galaxies: star formation – turbulence

Online-only material: color figures

1. INTRODUCTION

Star formation is regulated by many physical factors, with processes from sub-parsec to super-kiloparsec scales contributing to setting the overall rate (see, e.g., McKee & Ostriker 2007). One of the key factors expected to control the star formation rate is the available supply of gas. Over the whole range of star-forming systems, from entire spiral galaxies to circumnuclear starbursts, the global average of the surface density of star formation, $\Sigma_{\rm SFR}$, is observed to be correlated with the global average of the neutral gas surface density Σ as $\Sigma_{\rm SFR} \propto \Sigma^{1+p}$ with $1 + p \approx 1.4$ (Kennicutt 1998). Recent observations at high spatial resolution have made it possible to investigate local, rather than global, correlations of the star formation rate with Σ, using either azimuthal averages over rings, or mapping with apertures down to $\lesssim$ kpc scales (e.g., Wong & Blitz 2002; Boissier et al. 2003, 2007; Heyer et al. 2004; Komugi et al. 2005; Schuster et al. 2007; Kennicutt et al. 2007; Dong et al. 2008; Bigiel et al. 2008; Blanc et al. 2009; Verley et al. 2010). While power-law (Schmidt 1959, 1963) relationships are still evident in these local studies, steeper slopes are found for the outer, atomic-dominated regions of spiral galaxies (as well as dwarf galaxies) compared to the inner, molecular-dominated regions of spirals. In addition, measured indices in the low-Σ, low-$\Sigma_{\rm SFR}$ regime vary considerably from one galaxy to another. Thus, no single Schmidt law characterizes the regulation of star formation on local scales in the outer parts of galaxies.

The nonlinearity of observed Schmidt laws implies that not just the quantity of gas, but also its physical state and the surrounding galactic environment, affect the star formation rate. Indices $p > 0$ imply that the star formation efficiency is higher in higher-density regions, which are generally nearer the centers of galaxies and have shorter dynamical times. Indeed, the expectation based on theory and numerical simulations (Goldreich & Lynden-Bell 1965; Kim & Ostriker 2001) in thin, single-phase gaseous disks is that gravitational instabilities leading to star formation would grow only if the Toomre parameter (Toomre 1964) $Q \equiv v_{\rm th}\kappa/(\pi G\Sigma)$ is sufficiently small. These instabilities would develop over a timescale comparable to the galactic orbital time $t_{\rm orb} \equiv 2\pi/\Omega$, which corresponds to about twice the two-dimensional Jeans time $t_{J,2D} \equiv v_{\rm th}/(G\Sigma)$ when Q is near critical. Here, $v_{\rm th}$ is the thermal speed ($v_{\rm th}^2 \equiv P_{\rm th}/\rho = kT/\mu$ for $P_{\rm th}$, ρ, and T the gas thermal pressure, density, and temperature), and κ is the epicyclic frequency ($\kappa^2 \equiv R^{-3}d\Omega^2/dR$). While the implied scaling $\Sigma_{\rm SFR} \propto \Sigma\Omega$ is roughly satisfied globally (Kennicutt 1998), supporting the notion that galaxies evolve toward states with Q roughly near critical (e.g., Quirk 1972), for more local observations this does not provide an accurate prediction of star formation (e.g., Leroy et al. 2008; Wong 2009).

In addition to galactic rotation and shear rates, an important aspect of local galactic environment is the gravity of the stellar component. The background stellar gravity compresses the disk vertically (affecting the three-dimensional Jeans time $t_J \equiv$

[5] Hubble Fellow.

$\sqrt{\pi/(G\rho)}$), and perturbations in the stellar density can act in concert with gaseous perturbations in gravitational instabilities (altering the effective Q). Thus, one might expect the stellar surface density Σ_s and/or volume density ρ_s to affect the star formation rate (see, e.g., Kim & Ostriker 2007 and references therein). For example, if the stellar vertical gravity dominates that of the gas (see Section 2 for a detailed discussion of this), a scaling $\Sigma_{\rm SFR} \propto \Sigma/t_J$ would imply $\Sigma_{\rm SFR} \propto \Sigma^{3/2}(G^3\rho_s)^{1/4}/v_{\rm th}$ for a constant-temperature gas disk. Although star formation does appear to be correlated with Σ_s (e.g., Ryder & Dopita 1994; Hunter et al. 1998; see also below), the simple scaling $\propto \Sigma/t_J$ (taking into account both gaseous and stellar gravity, and assuming constant $v_{\rm th}$, in calculating t_J) does not in fact provide an accurate local prediction of star formation rates (e.g., Abramova & Zasov 2008; Leroy et al. 2008; Wong 2009).

A likely reason for the inaccuracy of the simple star formation prescriptions described above is that they do not account for the multiphase character of the interstellar medium (ISM), in which most of the volume is filled with low-density warm (or hot) gas but much (or even most) of the mass is found in clouds at densities two or more orders of magnitude greater than that of the intercloud medium. For the colder (atomic and molecular) phases, the turbulent velocity dispersions are much larger than $v_{\rm th}$, so that the mean gas density $\bar{\rho}$ averaged over the disk thickness depends on the turbulent vertical velocity dispersion. Even when multiphase gas and turbulence (and stellar and gas gravity) are taken into account in simulations, the simple estimate $\Sigma_{\rm SFR} \propto \Sigma/t_J \propto \Sigma\sqrt{G\bar{\rho}}$ (using $\bar{\rho}$ directly measured from the simulations) yields Schmidt-law indices steeper than the true values measured in both the simulations and in real galaxies (Koyama & Ostriker 2009a). Perhaps this should not be surprising, since one would expect the proportions of gas among different phases, as well as the overall vertical distribution, to affect the star formation rate. If, for example, most of the ISM's mass were in clouds of fixed internal density that formed stars at a fixed rate, then increasing the vertical velocity dispersion of this system of clouds would lower $\bar{\rho}$ but leave $\Sigma_{\rm SFR}$ unchanged.

The relative proportions of gas among different phases seems difficult to calculate from first principles, because it depends on how self-gravitating molecular clouds form and how they are destroyed, both of which are very complex processes. Intriguingly, however, analysis of recent observations of spiral galaxies has shown that the surface density of the molecular component averaged over $\sim$ kiloparsec annuli or local patches shows a relatively simple overall behavior, increasing roughly linearly with the empirically estimated midplane gas pressure (Wong & Blitz 2002; Blitz & Rosolowsky 2004, 2006; Leroy et al. 2008). The physical reason behind this empirical relation has not, however, yet been explained.

In this paper, we use a simple physical model to analyze how the gas is partitioned into diffuse and self-gravitating components, based on considerations of dynamic and thermodynamic equilibrium. We develop the idea that the midplane pressure in the diffuse component must simultaneously satisfy constraints imposed by vertical force balance, and by balance between heating (primarily from UV) and cooling. In particular, we propose that the approximately linear empirical relation between molecular content and midplane pressure identified by Blitz & Rosolowsky (2004, 2006) arises because the equilibrium gas pressure is approximately proportional to the UV heating rate; since the mean UV intensity is proportional to the star formation rate and the star formation rate is proportional to the molecular mass in normal spirals, the observed relationship naturally emerges.[6] We use our analysis to predict the dependence of the star formation rate on the local gas, stellar, and dark matter content of disks, and compare our predictions with observations. The analysis, including our basic assumptions and observational motivation for parameters that enter the theory, is set out in Section 2. Section 3 then compares to the observed data set previously presented in Leroy et al. (2008). In Section 4, we summarize and discuss our main results.

2. ANALYSIS

2.1. Model Concepts and Construction

In this section, we construct a local steady-state model for the star formation rate in the disk, with independent variables the total surface density of neutral gas (Σ), the midplane stellar density (ρ_s), and the dark matter density ($\rho_{\rm dm}$). The latter two quantities enter only through their effect on the vertical gravitational field. To develop this model, we suppose that the diffuse gas filling most of the volume of the ISM is in an equilibrium state. The equilibrium in the diffuse ISM has two aspects: force balance in the vertical direction (with a sum of pressure forces offsetting a sum of gravitational forces), and balance between heating and cooling (where heating is dominated by the FUV). Star-forming clouds, because they are self-gravitating entities at much higher pressure than their surroundings, are treated as separate from the space-filling diffuse ISM. The abundance of gravitationally bound, star-forming clouds is nevertheless important for establishing an equilibrium state in the diffuse gas, because the FUV that heats the diffuse ISM originates in young OB associations. We assume (consistent with observations and numerical simulations) that the equilibrium thermal state established for the diffuse medium includes both warm and cold atomic gas. This hypothesis leads to a connection between the dynamical equilibrium state and the thermal equilibrium state: there are two separate constraints on the pressure that must be simultaneously satisfied. These conditions are met by an appropriate partition of the available neutral gas into diffuse and self-gravitating components.

The reason for the partition between diffuse and self-gravitating gas can be understood by considering the physical requirements for equilibrium. The specific heating rate (Γ) in the diffuse gas is proportional to the star formation rate, which is proportional to the amount of gas that has settled out of the vertically dispersed diffuse gas and collected into self-gravitating clouds. The specific cooling rate ($n\Lambda$) in the diffuse gas is proportional to the density and hence to the thermal pressure, which (if force balance holds) is proportional to the vertical gravity and to the total surface density of diffuse gas. Thus, an equilibrium state, in which cooling balances heating and pressure balances gravity, can be obtained by a suitable division of the gas mass into star-forming (gravitationally bound) and diffuse components such that their ratio is proportional to the vertical gravitational field. If too large a fraction of the total surface density is in diffuse gas, the pressure will be too high, while the star formation rate will be too low. In this situation, the cooling would exceed heating, and mass would "drop out" of the diffuse component to produce additional star-forming gas. With additional star formation, the FUV intensity would raise the heating rate in the diffuse gas until it matches the cooling.

[6] Dopita (1985) previously showed that assuming the pressure to be proportional to the star formation rate yields scaling properties similar to observed relationships.

In the remainder of this section, we formalize these ideas mathematically, first defining terms (Section 2.2), then considering the requirements of dynamical balance (Section 2.3) and thermal balance (Section 2.4), and finally combining these to obtain an expression for the star formation rate when both equilibria are satisfied (Section 2.5). We then discuss, from a physical point of view, how the various feedback processes might act to adjust the system over time, steering it toward the equilibrium we have identified (Section 2.6). While evolving to an equilibrium of this kind is plausible, we emphasize that this is an assumption of the present model, which must be tested by detailed time-dependent simulations.[7] A worked example applying the model to an idealized galaxy is presented in Section 2.7. In developing the present model, we have adopted a number of simplifications that a more refined treatment should address; we enumerate several of these issues in Section 2.8.

2.2. Gas Components

In this model, we divide the neutral ISM into two components. One component consists of the gas that is collected into gravitationally bound clouds (GBCs) localized near the galactic midplane, with mean surface density (averaged over $\sim$ kpc scales) of $\Sigma_{\rm GBC}$. The other component consists of gas that is diffuse (i.e., not gravitationally bound), with mean surface density $\Sigma_{\rm diff}$. Here, we use the term "diffuse" in the sense of being widely dispersed or scattered throughout the volume; the diffuse component may include both tenuous, volume-filling gas and small, dense cloudlets (see below). All star formation is assumed to take place within the GBC component. In normal galaxies, the GBC component is identified with the population of giant molecular clouds (GMCs). Note that while observed GMCs in the Milky Way consist primarily of molecular gas, they also contain atomic gas in shielding layers. More generally, as we shall discuss further below, the relative proportions of molecular and dense atomic gas in GBCs depends on the cloud column and metallicity, and GBCs could even be primarily atomic if the metallicity is sufficiently low.

The diffuse component is identified (in normal galaxies) with the atomic ISM. We treat the diffuse gas as a two-phase cloud–intercloud medium in thermal pressure equilibrium, with turbulent vertical velocity dispersion v_z^2 assumed to be the same for warm and cold phases. Although the cold cloudlets within the diffuse component have much higher internal density than the warm intercloud gas, they are (by definition) each of sufficiently low mass that they are non-self-gravitating, such that their thermal pressure (approximately) matches that of their surroundings. The pressure in the interior of GBCs is considerably higher than the pressure of the surrounding diffuse gas (cf. Koyama & Ostriker 2009b).

In reality, the diffuse gas would not have a single unique pressure even if the radiative heating rate is constant because of time-dependent dynamical effects: turbulent compressions and rarefactions heat and cool the gas, altering what would otherwise be a balance between radiative heating and cooling processes. Nevertheless, simulations of turbulent gas with atomic-ISM heating and cooling indicate that the majority of the gas has pressure within $\sim$50% of the mean value (Piontek & Ostriker 2005, 2007), although the breadth of the pressure peak depends on the timescale of turbulent forcing $\sim L_{\rm turb}/v_{\rm turb}$ compared to the cooling time (Audit & Hennebelle 2005, 2010; Hennebelle & Audit 2007; Gazol et al. 2005, 2009; Joung & Mac Low 2006; Joung et al. 2009). Observations indicate a range of pressures in the cold atomic gas in the solar neighborhood, with a small fraction of the gas at very high pressures, and $\sim$50% of the gas at pressures within $\sim$50% of the mean value (Jenkins & Tripp 2001, 2007).

In general, the volume-weighted mean thermal pressure at the midplane is given by

$$\langle P_{\rm th}\rangle_{\rm vol} = \frac{\int P_{\rm th} d^3x}{\int d^3x} = \frac{\int (P_{\rm th}/\rho)\rho d^3x}{\int d^3x} = \frac{\int \rho d^3x}{\int d^3x}\frac{\int v_{\rm th}^2 dm}{\int dm} = \rho_0 \langle v_{\rm th}^2\rangle_{\rm mass}, \quad (1)$$

where ρ_0 is the volume-weighted mean midplane density of diffuse gas. The quantity $\langle v_{\rm th}^2\rangle_{\rm mass}$ is the mass-weighted mean thermal velocity dispersion; for a medium with warm and cold gas with respective mass fractions (in the diffuse component) f_w and $f_c = 1 - f_w$ and temperatures T_w and T_c,

$$\frac{\langle v_{\rm th}^2\rangle_{\rm mass}}{c_w^2} = f_w + \frac{T_c}{T_w}(1 - f_w) \equiv \tilde{f}_w. \quad (2)$$

Here, $c_w \equiv (P_w/\rho_w)^{1/2} = (kT_w/\mu)^{1/2}$ is the thermal speed of warm gas. Since the ratio T_w/T_c is typically $\sim$100, $\tilde{f}_w \approx f_w$ unless f_w is extremely small.

If the thermal pressures in the warm and cold diffuse-gas phases are the same, $\langle P_{\rm th}\rangle_{\rm vol} = P_w = \rho_w c_w^2$, so that from Equations (1) and (2),

$$\frac{\rho_w}{\rho_0} = \frac{\langle v_{\rm th}^2\rangle_{\rm mass}}{c_w^2} = \tilde{f}_w. \quad (3)$$

This result still holds approximately even if the warm and cold medium pressures differ somewhat, since the warm gas fills most of the volume, $\langle P_{\rm th}\rangle_{\rm vol} \approx P_w$. Note that one can also write $\rho_w/\rho_0 = f_w(V_{\rm tot}/V_w)$ for $V_{\rm tot}$ and V_w the total and warm-medium volumes, so that $\tilde{f}_w \approx f_w$ provided the warm medium fills most of the volume. If the medium is all cold gas, $\tilde{f}_w = T_c/T_w$. Henceforth, we shall assume the warm and cold gas pressures are equal at the midplane so that $\langle P_{\rm th}\rangle_{\rm vol} \to P_{\rm th}$; for convenience, we shall also omit the subscript on $\langle v_{\rm th}^2\rangle_{\rm mass}$.

2.3. Vertical Dynamical Equilibrium of Diffuse Gas

By averaging the momentum equation of the diffuse component horizontally and in time, and integrating outward from the midplane, it is straightforward to show that the difference in the total vertical momentum flux across the disk thickness (i.e., between midplane and $z_{\rm diff,max}$) must be equal to the total weight of the diffuse gas (e.g., Boulares & Cox 1990; Piontek & Ostriker 2007; Koyama & Ostriker 2009b). This total weight has three terms. The first term is the weight of the diffuse gas in its own gravitational field,

$$\int_0^{z_{\rm diff,max}} \rho \frac{d\Phi_{\rm diff}}{dz} dz = \frac{1}{8\pi G}\int_0^{z_{\rm diff,max}} \frac{d\left(\frac{d\Phi_{\rm diff}}{dz}\right)^2}{dz} dz = \frac{\pi G \Sigma_{\rm diff}^2}{2}, \quad (4)$$

where we have used $|d\Phi_{\rm diff}/dz|_{z_{\rm diff,max}} = 2\pi G\Sigma_{\rm diff}$ for a slab. The second term is the weight of the diffuse gas in the mean gravitational field associated with the GBCs,

$$\int_0^{z_{\rm diff,max}} \rho \frac{d\Phi_{\rm GBC}}{dz} dz \approx \pi G \Sigma_{\rm GBC}\Sigma_{\rm diff}, \quad (5)$$

[7] Very recent numerical studies provide support for the quasi-equilibrium assumption—see C.-G. Kim et al. (2010, in preparation).

where we have assumed that the scale height of the GBC distribution is much smaller than that of the diffuse gas so that $|d\Phi_{\rm GBC}/dz| \approx 2\pi G\Sigma_{\rm GBC}$ over most of the integral. Note that Equation (5) gives an upper bound on this term in the weight, with a lower bound given by $\pi G\Sigma_{\rm GBC}\Sigma_{\rm diff}/2$, corresponding to the case in which the vertical distributions of the diffuse and gravitationally bound components are the same. The third term is the weight in the gravitational field associated with the disk stars plus dark matter,

$$\int_0^{z_{\rm diff,max}} \rho\left(\frac{d\Phi_{\rm s}}{dz}+\frac{d\Phi_{\rm dm}}{dz}\right)dz \equiv 2\pi\zeta_d G\frac{\rho_{\rm sd}\Sigma_{\rm diff}^2}{\rho_0}. \quad (6)$$

Here, $\rho_{\rm sd} = \rho_s + \rho_{\rm dm}$ is the midplane density of the stellar disk plus that of the dark matter halo; we have assumed a flat rotation curve $V_c = $ const for the dark halo so that $\rho_{\rm dm} = (V_c/R)^2/(4\pi G)$.[8] The stellar disk's scale height is assumed to be larger than that of the diffuse gas, so that $g_z \approx 4\pi G\rho_{\rm sd}z$ within the diffuse-gas layer. The numerical value of ζ_d depends, but not sensitively, on the exact vertical distribution of the gas, which in turn depends on whether self- or external gravity dominates; $\zeta_d \approx 0.33$ within 5% for a range of cases between zero external gravity and zero self gravity. Allowing for a gradient in the vertical stellar density within the gas distribution, the stellar contribution to the weight would be reduced by a factor $\sim 1 - (2/3)(H_g/H_s)^2$, where H_g and H_s are the gaseous and stellar scale heights. In the (unlikely) circumstance that the diffuse-gas scale height is much larger than that of the stars, $g_z \approx 2\pi G\Sigma_s$ would be substituted for the gravity of the stellar component, yielding a contribution analogous to that in Equation (5) with $\Sigma_{\rm GBC} \rightarrow \Sigma_s$.

Including both thermal and kinetic terms, and taking $\rho \rightarrow 0$ at the top of the diffuse-gas layer, the difference in the gaseous vertical momentum flux between $z = 0$ and $z_{\rm diff,max}$ is given by $P_{\rm th} + \rho_0 v_z^2$. The term v_z^2 is formally a mass-weighted quantity (analogous to $\langle v_{\rm th}^2\rangle_{\rm mass}$), but we assume a similar turbulent velocity dispersion for the diffuse warm and cold atomic gas (Heiles & Troland 2003). If the magnetic field is significant, a term equal to the difference between $B^2/(8\pi) - B_z^2/(4\pi)$ at $z = 0$ and $z_{\rm diff,max}$ is added (Boulares & Cox 1990; Piontek & Ostriker 2007). Like other pressures, these magnetic terms are volume weighted; both observations (Heiles & Troland 2005) and numerical simulations (Piontek & Ostriker 2005) indicate that field strengths in the warm and cold atomic medium are similar. If the scale height of the magnetic field is larger than that of the diffuse gas (as some observations indicate; see, e.g., Ferrière 2001), then this term will be small, while it will provide an appreciable effect if $B \rightarrow 0$ where $\rho \rightarrow 0$. In any case, the magnetic term in the vertical momentum flux may be accounted for by taking $\rho_0 v_z^2 \rightarrow \rho_0 v_z^2 + (\Delta B^2/2 - \Delta B_z^2)/4\pi \equiv \rho_0 v_t^2$, where Δ indicates the difference between values of the squared magnetic field at $z = 0$ and $z_{\rm diff,max}$. Cosmic rays have a much larger scale height than that of the diffuse (neutral) gas, such that difference in the cosmic-ray pressure between $z = 0$ and $z_{\rm diff,max}$ may be neglected. We have also neglected the contribution from diffuse warm ionized gas, which has a low mean density and large scale height compared to that of the neutral gas (e.g., Gaensler et al. 2008).

Equating the momentum flux difference with the total weight, we have

$$P_{\rm th}\left(1+\frac{v_t^2}{c_w^2\tilde{f}_w}\right) = \frac{\pi G}{2}\Sigma_{\rm diff}^2 + \pi G\Sigma_{\rm GBC}\Sigma_{\rm diff} + 2\pi\zeta_d G c_w^2\tilde{f}_w\frac{\rho_{\rm sd}\Sigma_{\rm diff}^2}{P_{\rm th}}. \quad (7)$$

Here, we have used Equations (1) and (2) to substitute $\tilde{f}_w c_w^2/P_{\rm th}$ for ρ_0^{-1} on the right-hand side. As noted above, the second term on the right-hand side could be reduced by up to a factor of two, if the scale height of the GBC distribution approaches that of the diffuse gas. It is convenient to define

$$\alpha \equiv 1+\frac{v_t^2}{c_w^2\tilde{f}_w} = \frac{\langle v_{\rm th}^2\rangle + v_t^2}{\langle v_{\rm th}^2\rangle} = \frac{P_{\rm th} + \rho_0 v_z^2 + \Delta\left(B^2/2 - B_z^2\right)/(4\pi)}{P_{\rm th}}, \quad (8)$$

which represents the midplane ratio of total effective pressure to thermal pressure. If the magnetic contribution is small (which would be true if $\Delta B^2 \ll B^2$, even if magnetic and thermal pressures are comparable at the midplane), α is the total observed velocity dispersion σ_z^2 divided by the mean thermal value. We shall treat v_t, c_w, and $\tilde{f}_w$ as parameters that do not vary strongly within a galaxy or from one galaxy to another (see below), and $\Sigma_{\rm diff}$, $\Sigma_{\rm GBC}$, and $P_{\rm th}$ as (interdependent) variables. At any location in a galaxy, we shall consider $\rho_{\rm sd}$ (and the total gas surface density $\Sigma = \Sigma_{\rm diff} + \Sigma_{\rm GBC}$) as a given environmental conditions.

Equation (7) is a quadratic in both $\Sigma_{\rm diff}$ and $P_{\rm th}$. Thus, if $P_{\rm th}$ and $\Sigma_{\rm GBC}$ are known, we may solve to obtain the surface density of diffuse gas:

$$\Sigma_{\rm diff} = \frac{2\alpha P_{\rm th}}{\pi G\Sigma_{\rm GBC} + \left[(\pi G\Sigma_{\rm GBC})^2 + 2\pi G\alpha\left(P_{\rm th} + 4\zeta_d c_w^2\tilde{f}_w\rho_{\rm sd}\right)\right]^{1/2}}. \quad (9)$$

Scaling the variables to astronomical units, the result in Equation (9) can also be expressed as

$$\Sigma_{\rm diff} = \left\{9.5\,M_\odot\ {\rm pc}^{-2}\alpha\left(\frac{P_{\rm th}/k}{3000\ {\rm K\,cm^{-3}}}\right)\right\} \times \left\{0.11\left(\frac{\Sigma_{\rm GBC}}{1\,M_\odot\ {\rm pc}^{-2}}\right) + \left[0.011\left(\frac{\Sigma_{\rm GBC}}{1\,M_\odot\ {\rm pc}^{-2}}\right)^2 + \alpha\left(\frac{P_{\rm th}/k}{3000\ {\rm K\,cm^{-3}}}\right) + 10\alpha\tilde{f}_w\left(\frac{\rho_{\rm sd}}{0.1\,M_\odot\ {\rm pc}^{-3}}\right)\right]^{1/2}\right\}^{-1}. \quad (10)$$

What are appropriate parameter values to use? Since thermal balance in the warm medium is controlled by line cooling (Wolfire et al. 1995, 2003), the warm-medium temperature is relatively insensitive to local conditions in a galaxy; we shall adopt $c_w = 8$ km s^{-1}. Numerical simulations in multiphase

[8] If the vertical stellar distribution in the disk varies as $\rho_s \propto {\rm sech}^2(z/H_s)$ with $H_s = v_{z,s}^2/(\pi G\Sigma_s)$, then the midplane stellar density is $\rho_s = \Sigma_s/(2H_s) = \pi G\Sigma_s^2/(2v_{z,s}^2)$. Existing photometric and kinematic observations suggest that $H_s \sim$ const and $v_{z,s} \propto \Sigma_s^{1/2}$ (van der Kruit & Searle 1982; Bottema 1993), but these are sensitive primarily to the central parts of the disk. Note that if the Toomre parameter for the stellar disk and the vertical-to-horizontal velocity dispersion ratio are both constant with radius, then $\rho_s \propto \rho_{\rm dm} \propto (V_c/R)^2$. In this case, the ratio of the gas-to-stellar scale height is $\sim v_{z,g}/v_{z,s}$; since the gas can dissipate turbulence and cool to maintain constant $v_{z,g}$ while the stellar velocity dispersion secularly increases over time, the gas layer will tend to be thinner than the stellar layer even if both components flare in the outer parts of galaxies.

gas have shown that the magnetic field is amplified by the magnetorotational instability to a level $B^2/(8\pi) = (1-2)P_{\rm th}$, independent of the mass fractions of cold and warm gas and the vertical gravitational field strength (Piontek & Ostriker 2005, 2007), while $|B_z/B_\phi| \ll 1$. This is consistent with observed magnetic field strengths measured in the Milky Way and in external galaxies (Heiles & Troland 2005; Beck 2008). Large-scale turbulent velocity dispersions observed in local H I gas (both warm and cold) are $\sim$7 km s^{-1}, comparable to c_w (Heiles & Troland 2003; Mohan et al. 2004). Total vertical velocity dispersions in H I gas in external galaxies are also observed to be in the range 5–15 km s^{-1}, decreasing outward from the center (Tamburro et al. 2009).

The most uncertain parameter is $\tilde{f}_w \approx f_w$, the fraction of the diffuse mass in the warm phase. In the solar neighborhood, this is $\sim$0.6 (Heiles & Troland 2003), and in external galaxies the presence of both narrower and broader components of 21 cm emission suggests that both warm and cold gas are present (de Blok & Walter 2006), with some indication based on "universality" in line profile shapes that the warm-to-cold mass ratio does not strongly vary with position (Petric & Rupen 2007). In the outer Milky Way, the ratio of H I emission to absorption appears nearly constant out to $\sim$25 kpc, indicating that the warm-to-cold ratio does not vary significantly (Dickey et al. 2009). In dwarf galaxies as well, observations indicate that both a cold and warm H I component is present (Young & Lo 1996). While uncertain, it is likely that $\tilde{f}_w \sim 0.5$–1, at least in outer galaxies.

Thus, allowing for the full range of observed variation, $\alpha \sim 2$–10, $\alpha\tilde{f}_w \sim 1$–5, and $\alpha/\tilde{f}_w \sim 2$–20; we shall adopt $\alpha = 5$ and $\tilde{f}_w = 0.5$ as typical for mid-to-outer-disk conditions. For these fiducial parameters, and taking midplane thermal pressure $P_{\rm th,0}/k \sim 3000$ K cm^{-3} (see Jenkins & Tripp 2001 and Wolfire et al. 2003), $\rho_{\rm sd} = 0.05\,M_\odot$ pc^{-3} (Holmberg & Flynn 2000), and $\Sigma_{\rm GBC} \lesssim 2\,M_\odot$ pc^{-2} (Dame et al. 1987, 2001; Bronfman et al. 1988; Luna et al. 2006; Nakanishi & Sofue 2006) near the Sun, the result from Equation (10) is consistent with the observed total surface density estimate $\sim 10\,M_\odot$ pc^{-2} of atomic gas in the solar neighborhood (Dickey & Lockman 1990; Kalberla & Kerp 2009).

Equation (7) may also be solved to obtain the thermal pressure in terms of $\Sigma_{\rm diff}$, $\Sigma_{\rm GBC}$, $\rho_{\rm sd}$ and the diffuse-gas parameters α and $\tilde{f}_w$:

$$P_{\rm th} = \frac{\pi G\Sigma_{\rm diff}^2}{4\alpha}\left\{1+2\frac{\Sigma_{\rm GBC}}{\Sigma_{\rm diff}} + \left[\left(1+2\frac{\Sigma_{\rm GBC}}{\Sigma_{\rm diff}}\right)^2 + \frac{32\zeta_d c_w^2 \tilde{f}_w \alpha}{\pi G}\frac{\rho_{\rm sd}}{\Sigma_{\rm diff}^2}\right]^{1/2}\right\}. \quad (11)$$

Over most of the disk in normal galaxies, the term in Equation (11) that is proportional to $\rho_{\rm sd}$ (arising from the weight in the stellar-plus-dark-matter gravitational field) dominates; this yields

$$P_{\rm th} \sim \Sigma_{\rm diff}\,(2G\rho_{\rm sd})^{1/2}\left(\frac{\pi\zeta_d\tilde{f}_w}{\alpha}\right)^{1/2} c_w. \quad (12)$$

For given $\rho_{\rm sd}$ and Σ, the thermal pressure therefore increases approximately proportional to the fraction of gas in the diffuse phase, $f_{\rm diff} \equiv \Sigma_{\rm diff}/\Sigma$. With $(\pi\zeta_d)^{1/2} \approx 1$ and $\tilde{f}_w \approx f_w$, $P_{\rm th} \sim \Sigma_w\,(2G\rho_{\rm sd})^{1/2}\,c_w^2/(\langle v_{\rm th}^2\rangle + v_t^2)^{1/2}$ in this limit; i.e., it is the surface density of the volume-filling warm medium that sets the thermal pressure. Multiplying Equation (12) by α and using $\alpha\tilde{f}_w = (\langle v_{\rm th}^2\rangle + v_t^2)/c_w^2$ yields

$$P_{\rm tot} \sim \Sigma_{\rm diff}\,(2G\rho_{\rm sd})^{1/2}\left(\left\langle v_{\rm th}^2\right\rangle + v_t^2\right)^{1/2}. \quad (13)$$

This is the same as the formula for midplane pressure adopted by Blitz & Rosolowsky (2004, 2006), except that instead of $\Sigma_{\rm diff}$ their expression contains the total gas surface density Σ, instead of $(\langle v_{\rm th}^2\rangle + v_t^2)^{1/2}$ they use the thermal+turbulent vertical velocity dispersion (these are equal if vertical magnetic support is negligible), and they omit the dark matter contribution to $\rho_{\rm sd}$. Using $\rho_s = \pi G\Sigma_s^2/(2v_{z,s}^2)$ and taking $\Sigma_{\rm GBC}$, $\rho_{\rm dm} \to 0$, Equation (11) yields

$$P_{\rm tot} \sim \frac{\pi G\Sigma^2}{2}\left(1+\frac{\left[\left\langle v_{\rm th}^2\right\rangle + v_t^2\right)^{1/2}\right]^{1/2}\Sigma_s}{v_{z,s}\Sigma}\right), \quad (14)$$

recovering the result of Elmegreen (1989; except that he includes the total B^2, rather than ΔB^2, in v_t^2 and $P_{\rm tot}$).

2.4. Thermal Equilibrium of Diffuse Gas

As expressed by Equation (11), the thermal pressure in the diffuse gas must respond to the dynamical constraint imposed by vertical momentum conservation in the disk. In addition, the thermal pressure is also regulated by the microphysics of heating and cooling. Namely, if the atomic gas is in the two-phase regime (as is expected in a star-forming region of a galaxy; see Section 2.5), then the thermal pressure must lie between the minimum value for which a cold phase is possible, $P_{\rm min,cold}$, and the maximum value for which a warm phase is possible, $P_{\rm max,warm}$. Wolfire et al. (2003) found, based on detailed modeling of heating and cooling in the solar neighborhood, that geometric mean of these two equilibrium extrema, $P_{\rm two\text{-}phase} \equiv (P_{\rm min,cold}P_{\rm max,warm})^{1/2}$, is comparable to the local empirically estimated thermal pressure, and that two phases are expected to be present in the Milky Way out to $\sim$ 18 kpc. Based on turbulent numerical simulations with a bistable cooling curve, Piontek & Ostriker (2005, 2007) found that the mean midplane pressure evolves to a value near the geometric mean pressure $P_{\rm two\text{-}phase}$, for a wide range of vertical gravitational fields and warm-to-cold mass fractions. Thus, we expect the midplane thermal pressure in the diffuse gas to be comparable to the two-phase value defined by the thermal equilibrium curve, $P_{\rm th} \approx P_{\rm two\text{-}phase}$. Since $P_{\rm max,warm}/P_{\rm min,cold} \sim 2$–5 (Wolfire et al. 2003), even if $P_{\rm th} = P_{\rm two\text{-}phase}$ does not hold precisely, the midplane pressure $P_{\rm th}$ will be within a factor ~ 2 of $P_{\rm two\text{-}phase}$ provided the diffuse gas is in the two-phase regime.

For the fiducial solar-neighborhood model of Wolfire et al. (2003), the geometric mean thermal pressure is $P_{\rm two\text{-}phase}/k \sim P_{\rm th,0}/k \sim 3000$ K cm^{-3}. For other environments, the values of $P_{\rm min,cold}$ and $P_{\rm max,warm}$ depend on the heating of the gas: enhanced heating pushes the transition pressures upward (Wolfire et al. 1995). Because the dominant heating is provided by the photoelectric effect on small grains, $P_{\rm two\text{-}phase}$ increases approximately linearly with the FUV intensity. Assuming that $P_{\rm two\text{-}phase}$ scales with $P_{\rm min,cold}$, we adapt the expression given in Wolfire et al. (2003) and normalize $P_{\rm two\text{-}phase}$ using the solar-neighborhood value:

$$\frac{P_{\rm two\text{-}phase}}{k} = 12{,}000\ {\rm K\,cm^{-3}}\,\frac{G_0'Z_d'/Z_g'}{1+3.1(G_0'Z_d'/\zeta_t')^{0.365}}. \quad (15)$$

Here, G_0' is the mean FUV intensity relative to the solar-neighborhood value $J_{\rm FUV,0} = 2.1\times10^{-4}$ erg cm^{-2} s^{-1}sr^{-1}, ζ_t' is equal to the total cosmic ray/EUV/X ray ionization rate relative to the value 10^{-16} s^{-1}, and Z_d' and Z_g' are, respectively, the dust and gas abundances relative to solar-neighborhood values.

The FUV is produced by OB associations, so that the intensity will be proportional to the star formation rate per unit surface area. The intensity also depends on the radiative transfer of the UV. For example, a slab of gas with UV optical depth $\tau_\perp = \kappa\Sigma$ and total surface density of FUV emission $\Sigma_{\rm FUV}$ has $J_{\rm FUV} = \Sigma_{\rm FUV}(1 - E_2(\tau_\perp/2))/(4\pi\tau_\perp)$, where E_2 is the second exponential integral. This correction for radiative transfer depends logarithmically on $1/\tau_\perp$ at low optical depth (yielding a variation $\propto R$ if Σ is an exponential—see Elmegreen & Parravano 1994), varying by $\sim$ 50% for $\tau_\perp \sim$ 0.1–1. For simplicity, we neglect variations in $J_{\rm FUV}$ associated with the radiative transfer here; we shall simply assume $J_{\rm FUV} \propto \Sigma_{\rm FUV} \propto \Sigma_{\rm SFR}$. Fuchs et al. (2009; see also Bertelli & Nasi 2001; Vergely et al. 2002) find that the solar-neighborhood value of the surface star formation rate $\Sigma_{\rm SFR,0}$ is $2.5\times10^{-9}\,M_\odot$ pc^{-2} yr^{-1}, which then yields

$$G_0' \equiv \frac{J_{\rm FUV}}{J_{\rm FUV,0}} \approx \frac{\Sigma_{\rm SFR}}{\Sigma_{\rm SFR,0}} = \frac{\Sigma_{\rm SFR}}{2.5\times10^{-9}\,M_\odot\ {\rm pc}^{-2}\ {\rm yr}^{-1}}. \quad (16)$$

Since Equation (15) is normalized using the observed solar-neighborhood pressure $P_{\rm th,0}$ and Equation (16) is normalized using the (inverse of the) observed solar-neighborhood star formation rate $\Sigma_{\rm SFR,0}$, our model depends only on the ratio of these quantities, $P_{\rm th,0}/\Sigma_{\rm SFR,0}$. Equivalently, since Wolfire et al. (2003) predict the value of $P_{\rm th,0}/J_{\rm FUV,0}$ from theory, our model depends on the measured ratio of local FUV intensity to local star formation rate, $J_{\rm FUV,0}/\Sigma_{\rm SFR,0}$. Although here we adopt an empirical value for $J_{\rm FUV}/\Sigma_{\rm SFR}$ based on the solar neighborhood, in principle this ratio may be calculated theoretically with a detailed radiative transfer and population synthesis model. Simple estimates using standard relationships between the FUV emission and $\Sigma_{\rm SFR}$ (e.g., Salim et al. 2007) yield values of $J_{\rm FUV}/\Sigma_{\rm SFR}$ similar to our adopted value from the solar neighborhood.

Assuming the high-energy ionization rate is proportional to the local value of $\Sigma_{\rm SFR}$ and inversely proportional to Σ (Wolfire et al. 2003),

$$\frac{G_0'}{\zeta_t'} = \frac{\Sigma}{\Sigma_0}, \quad (17)$$

where Σ_0 is the surface density of neutral gas at the solar circle. Strictly speaking, the above would only apply to cosmic rays, with $\zeta_t' \propto \Sigma_{\rm diff}^{-1}$ instead of Σ^{-1} for soft X-rays and EUV. In practice, however, this does not affect the results for the star formation rate, since the dependence on this term is weak to begin with, and only enters the prediction for $\Sigma_{\rm SFR}$ in outer disks (see Equation (22)), where $\Sigma \to \Sigma_{\rm diff}$.

Taking $\Sigma_0 \sim 10\,M_\odot$ pc^{-2} and setting $Z_d'/Z_g' = 1$ yields, for $P_{\rm th} = P_{\text{two-phase}}$,

$$\Sigma_{\rm SFR} \approx 6\times10^{-10}\,M_\odot\ {\rm pc}^{-2}\ {\rm yr}^{-1}\left(\frac{P_{\rm th}/k}{3000\ {\rm K\,cm}^{-3}}\right) \times\left[1+3\left(\frac{Z_d'\Sigma}{10\,M_\odot\ {\rm pc}^{-2}}\right)^{0.4}\right]; \quad (18)$$

this can be combined with Equation (11) to yield a prediction for the star formation rate in terms of the gas and stellar contents of the disk. More generally, Equation (16) may be inserted into Equation (15), and the result substituted in Equation (9) or (11) to obtain, respectively, an expression for $\Sigma_{\rm diff}$ in terms of $\Sigma_{\rm SFR}$, $\rho_{\rm sd}$, and $\Sigma_{\rm GBC}$, or an expression for $\Sigma_{\rm SFR}$ in terms of $\Sigma_{\rm diff}$, $\rho_{\rm sd}$, and $\Sigma_{\rm GBC}$.

2.5. The Equilibrium Star Formation Rate

As our goal is to obtain a prediction for $\Sigma_{\rm SFR}$ in terms of the total gaseous surface density $\Sigma = \Sigma_{\rm diff} + \Sigma_{\rm GBC}$ and midplane stellar+dark-matter density $\rho_{\rm sd}$, we require an additional relationship among the variables. Since star formation is assumed to take place only within GBCs, if the timescale to convert this gas to stars is $t_{\rm SF,GBC}$, then

$$\Sigma_{\rm SFR} = \frac{\Sigma_{\rm GBC}}{t_{\rm SF,GBC}} = \frac{\Sigma - \Sigma_{\rm diff}}{t_{\rm SF,GBC}}. \quad (19)$$

In normal galaxies, GBCs are identified with GMCs (the outer layers of which are in fact atomic—see below). Recently, Bigiel et al. (2008) found that there is an approximately linear relationship between the molecular mass measured in CO and the star formation rate, over the mid-disk regions in a set of spiral galaxies where $\Sigma \sim$ 10–100 $M_\odot$ pc^{-2}. The measured proportionality constant is $t_{\rm SF,CO} \equiv \Sigma_{\rm mol,CO}/\Sigma_{\rm SFR} \approx 2\times10^9$ yr. Some recent studies targeting this regime in spirals at $\sim$ kiloparsec scales find weak systematic variations in $t_{\rm SF,CO}$ with surface density (Wong & Blitz 2002; Heyer et al. 2004; Kennicutt et al. 2007; Verley et al. 2010). These are mild (no more than a factor of 2–3 over the range Σ = 10–100 $M_\odot$ pc^{-2}) and almost all find a consistent normalization, with 2 Gyr being a typical timescale. CO is present only in the portions of clouds where $A_V \gtrsim 1$ (Wolfire et al. 2010; Glover & Mac Low 2010), so that it can become a poor tracer of molecular mass in low-metallicity systems. From observations of dust emission in the SMC, however, the star formation timescale in "dark" molecular gas (where hydrogen is in H_2 but carbon is atomic rather than in CO) is found to be similar to that in CO-bright gas (A. Bolatto 2010, private communication). Based on these empirical results, $t_{\rm SF,GBC} = t_{\rm SF,mol}\Sigma_{\rm GBC}/\Sigma_{\rm mol}$ for $t_{\rm SF,mol} \sim$ const.

Since GBCs contain both dense atomic shielding exteriors and dense molecular shielded interiors, while molecular gas may be both within GBCs and in unbound clouds, we can write

$$\frac{\Sigma_{\rm GBC}}{\Sigma_{\rm mol}} = \frac{M_{\rm mol,GBC} + M_{\rm atom,GBC}}{M_{\rm mol,GBC} + M_{\rm mol,diff}} = \frac{1 + (M_{\rm atom}/M_{\rm mol})_{\rm GBC}}{1 + \Sigma_{\rm mol,diff}/\Sigma_{\rm mol,GBC}}. \quad (20)$$

The atomic-to-molecular ratio within externally irradiated (spherical) clouds depends primarily on the metallicity and total cloud column density of hydrogen $N_{\rm H,cloud} \equiv M_{\rm cloud}/(\mu_H\pi R_{\rm cloud}^2)$ as $(M_{\rm atom}/M_{\rm mol})_{\rm cloud} \approx [Z'^{0.8}(N_{\rm H,cloud}/1.8\times10^{21}\,{\rm cm}^{-2}) - 0.7]^{-1}$ (Krumholz et al. 2009a; McKee & Krumholz 2010). Here, $N_{\rm H} = N_{\rm H\,I} + 2N_{\rm H_2}$. Assuming the column densities of GBCs are similar to the observed values $N_{\rm H,cloud} \sim 10^{22}$ cm^{-2} (i.e., $\Sigma_{\rm cloud} \sim 100\,M_\odot$ pc^{-2}) typical of star-forming clouds in the Milky Way and Local Group (e.g., Solomon et al. 1987; Sheth et al. 2008; Bolatto et al. 2008; Heyer

et al. 2009), we therefore have $(M_{\rm atom}/M_{\rm mol})_{\rm GBC} < 1$ except for low-metallicity environments $Z' < 0.2$. The regions of galaxies mapped in the Bigiel et al. (2008) sample have metallicity $Z' \gtrsim 0.5$, so clouds with $N_{\rm H,cloud} \sim 10^{22}\,{\rm cm}^{-2}$ would be mostly molecular. For clouds with this range of metallicity and column density such that $A_V \gtrsim 3$, most of the gas that is molecular (H_2 rather than H I) would also be observable in CO (Wolfire et al. 2010; Glover & Mac Low 2010). Assuming that for moderate values of Σ, most of the molecular gas is confined within GBCs, we also have $\Sigma_{\rm mol,diff}/\Sigma_{\rm mol,GBC} \ll 1$ (in galactic center regions where $\Sigma > 100\,M_\odot\ {\rm pc}^{-2}$, the diffuse molecular fraction may be larger). Thus, in the regime for which $t_{\rm SF,CO}$ is observed to be approximately constant, $\Sigma_{\rm GBC}/\Sigma_{\rm mol} \sim 1$ and $\Sigma_{\rm mol} \sim \Sigma_{\rm mol,CO}$, and we can then take $t_{\rm SF,GBC} \approx t_{\rm SF,mol} \approx t_{\rm SF,CO}$. Note that because CO is optically thick in clouds with $N_{\rm H,cloud} \sim 10^{22}\,{\rm cm}^{-2}$ and normal metallicity, observed CO emission in unresolved clouds may in fact trace the atomic and "dark gas" portions of GBCs as well as the regions where CO is present, because these contribute to the gravitational potential and therefore the total CO linewidth. To the extent that this is true (and provided there is minimal diffuse CO-emitting gas), $t_{\rm SF,CO}$ would be a direct measurement of $t_{\rm SF,GBC}$.

For the rest of this paper, we shall use $t_{\rm SF,GBC} \rightarrow t_{\rm SF} = {\rm const}$, and adopt the fiducial value of 2×10^9 yr based on Bigiel et al. (2008). Although the value we use for $t_{\rm SF,GBC}$ is calibrated from observations in which star-forming clouds are primarily molecular (and observable in CO lines), our basic approach would remain unchanged for GBCs in different parameter regimes, provided that a well-defined value of $t_{\rm SF,GBC}$ is known (from either observations with appropriate corrections for atomic and dark gas, or from theory). From a theoretical point of view, the internal dynamical properties of GBCs would be qualitatively similar whether they are mostly molecular or a mixture of cold atomic and molecular gas, but the value of $t_{\rm SF,GBC}$ would have to be adjusted to allow for the dependence of star formation efficiency on chemical content (see Section 2.8).

With the above assumptions, in Equation (9) we now can substitute $\Sigma_{\rm diff} = \Sigma - \Sigma_{\rm GBC}$ on the left-hand side, eliminate $P_{\rm th}$ in favor of $\Sigma_{\rm SFR}$ on the right-hand side using Equation (18) (or Equations (15)–(17)), and set $\Sigma_{\rm GBC} = t_{\rm SF}\Sigma_{\rm SFR}$. The result is an implicit expression for $\Sigma_{\rm SFR}$ in terms of Σ and $\rho_{\rm sd}$, which may be solved numerically. The Appendix provides a derivation of the expression for $\Sigma_{\rm SFR}$, given in Equations (A11) and (A12). Closed-form analytic solutions may be obtained in the limit of high and low values of the star formation rate. When $\Sigma_{\rm SFR}$ is high, the ISM is GBC dominated and $\Sigma_{\rm SFR} \approx \Sigma/t_{\rm SF}$. When $\Sigma_{\rm SFR}$ is low, the ISM is diffuse dominated. In this limit, $\Sigma_{\rm diff} \rightarrow \Sigma$ and we may drop $\Sigma_{\rm GBC}/\Sigma_{\rm diff}$ in Equation (11), resulting in

$$\frac{P_{\rm th,low}}{k} = \frac{1700\ {\rm K\,cm^{-3}}}{\alpha}\left(\frac{\Sigma}{10\,M_\odot\ {\rm pc}^{-2}}\right)^2 \times \left\{1 + \left[1 + 50\tilde{f}_w\alpha\frac{\left(\frac{\rho_{\rm sd}}{0.1\,M_\odot\ {\rm pc}^{-3}}\right)}{\left(\frac{\Sigma}{10\,M_\odot\ {\rm pc}^{-2}}\right)^2}\right]^{1/2}\right\}. \quad (21)$$

This result can then be inserted in Equation (18) to obtain a prediction for the dependence of $\Sigma_{\rm SFR}$ on $\rho_{\rm sd}$ and Σ in low-density outer-disk regions. An approximate form is

$$\Sigma_{\rm SFR,low} = 3 \times 10^{-10}\,M_\odot\ {\rm pc}^{-2}\ {\rm yr}^{-1}\left(\frac{\Sigma}{10\,M_\odot\ {\rm pc}^{-2}}\right) \times \left[1 + 3\left(\frac{Z'_d\Sigma}{10\,M_\odot\ {\rm pc}^{-2}}\right)^{0.4}\right] \times \left[\frac{2}{\alpha}\left(\frac{\Sigma}{10\,M_\odot\ {\rm pc}^{-2}}\right) + \left(\frac{50\tilde{f}_w}{\alpha}\right)^{1/2}\left(\frac{\rho_{\rm sd}}{0.1\,M_\odot\ {\rm pc}^{-3}}\right)^{1/2}\right] \quad (22)$$

(see also Equation (A13) in the Appendix). Note that the limit in Equation (22) applies in the solar neighborhood, where the stellar+dark-matter gravity (i.e., the term depending on $\rho_{\rm sd}$) accounts for 80% of the total contribution in second square bracket. An approximate form over the whole range $\Sigma \lesssim 100\,M_\odot\ {\rm pc}^{-2}$ is given by

$$\Sigma_{\rm SFR} \approx \left[\frac{t_{\rm SF}}{\Sigma} + \frac{1}{\Sigma_{\rm SFR,low}}\right]^{-1} \quad (23)$$

(see also Equation (A14) in the Appendix). In terms of the dependence on model parameters, at high surface density $\Sigma_{\rm SFR} \propto t_{\rm SF}^{-1}$, whereas at low surface density $\Sigma_{\rm SFR} \propto (\tilde{f}_w/\alpha)^{1/2}(\Sigma_{\rm SFR,0}/P_{\rm th,0})$.

2.6. Approach to Equilibrium

The above analysis yields a relation for the star formation rate in equilibrium, but how would the self-consistent state of dynamical, thermal, and star formation equilibrium be attained in a real galaxy? First, consider the timescales involved. Vertical dynamical equilibrium is reached on a timescale of a few times $\sim H/\sigma_z$, where σ_z is the vertical velocity dispersion. With $H \sim 100$ pc and $\sigma_z \sim 10$ km s^{-1}, this dynamical equilibrium is typically reached within a few times 10 Myr. Thermal equilibrium of diffuse gas at a given density is accomplished by a combination of heating and cooling; it is very fast in dense gas, and for low-density gas requires $\sim$5 Myr (Wolfire et al. 2003). Separation of the diffuse gas into phases, which involves dynamics and takes place via thermal instability, requires $\sim$20–50 Myr (Piontek & Ostriker 2004, 2005). The timescale for star formation to reach equilibrium depends on how GBCs are formed out of the diffuse gas; recent simulations (Koyama & Ostriker 2009a) suggest this may take a several tens of Myr for conditions similar to the solar circle (but without spiral structure). Thus, the slowest equilibrium to be established is likely that of the star formation rate, which depends on the relative proportions of diffuse and gravitationally bound gas. Because GBCs are continually forming and being destroyed within the disk (and material for a given GBC may be gathered horizontally from up to several H), at any time a given patch of the disk could be at a different point in this cycle. In an observed galaxy, measuring the equilibrium properties (for given Σ and $\rho_{\rm sd}$) would require averaging over a horizontal area large enough that the different states in the GBC formation–destruction cycle are represented.

As a (highly idealized) example of how the system might evolve, consider a region in which $f_{\rm diff} = \Sigma_{\rm diff}/\Sigma$ is initially high compared to the value in which all equilibrium conditions are satisfied. On the one hand, a higher-than-equilibrium $f_{\rm diff}$ implies a lower-than-equilibrium proportion of gas in star-forming bound clouds, yielding a value for $\Sigma_{\rm SFR} = (1 - f_{\rm diff})\Sigma/t_{\rm SF}$ lower than the level when overall equilibrium (including star

formation equilibrium) obtains. From Equations (15) and (16), when the radiation field is weak, the heating–cooling curve has a low values of $P_{\rm max,warm}$ and $P_{\rm min,cold}$ (and $P_{\rm two\text{-}phase}$). On the other hand, we would expect that within a few tens of Myr, thermal, dynamical, and phase equilibrium would be established with this (high) value of $\Sigma_{\rm diff}$. From Equation (11), if $\tilde{f}_w$ is constant, the midplane pressure in the diffuse gas in this situation would be higher than the value that would obtain when star formation equilibrium is satisfied (it can be shown algebraically from Equation (11) that $\partial P_{\rm th}/\partial f_{\rm diff} > 0$). Thus, for this situation with lower-than-equilibrium star formation rate (but other processes in equilibrium), the cooling equilibrium curve sits at a pressure lower than that in overall equilibrium, while the midplane pressure is higher than that in overall equilibrium.

Figure 1(a) shows an extreme case of higher-than-equilibrium $f_{\rm diff}$, in which the midplane pressure is higher than $P_{\rm max,warm}$. In this situation, a portion of the warm gas would condense to make cold clouds, lowering $\tilde{f}_w$ and reducing the midplane pressure. With a higher abundance of cold clouds, additional GBCs would form, lowering $f_{\rm diff}$, raising $\Sigma_{\rm SFR}$, and hence moving the thermal equilibrium curve toward higher pressure. As cold clouds are converted to GBCs, $\tilde{f}_w$ could return to its equilibrium value. But, with lower $f_{\rm diff}$ than in the initial situation, the midplane pressure would be reduced. The arrows in Figure 1(a) indicate how the midplane pressure and thermal equilibrium curve would evolve. This process would continue until a self-consistent state of thermal, dynamical, and star formation equilibrium, with $P_{\rm two\text{-}phase}$ comparable to the midplane pressure $P_{\rm th}$, is reached (see Figure 1(b)). (In fact, the midplane pressure $P_{\rm th}$ only needs to lie between $P_{\rm min,cold}$ and $P_{\rm max,warm}$, which allows a range of self-consistent equilibria; we discuss this issue below.)

As another example, we consider the opposite situation. We imagine a region with a bound-cloud proportion $1 - f_{\rm diff}$ and $\Sigma_{\rm SFR}/\Sigma$ above the self-consistent overall equilibrium values, such that heating associated with the high star formation rate makes the thermal equilibrium curve sit at high pressure (i.e., $P_{\rm two\text{-}phase}$ is high). With low $f_{\rm diff}$, $\Sigma_{\rm diff} = f_{\rm diff}\Sigma$ and the midplane diffuse-gas pressure will be low compared to the overall equilibrium (assuming constant $\tilde{f}_w$). Figure 1(c) illustrates an extreme of this situation, in which the heating rate is so high that cold atomic clouds would secularly heat and expand to increase the proportion of warm gas. The energy input to bound clouds associated with the high star formation rate would destroy GBCs at a faster rate than they could form, increasing $f_{\rm diff}$ and lowering $\Sigma_{\rm SFR}$ until a self-consistent equilibrium state (Figure 1(b)) is reached. The arrows indicate the evolution required move to a state in which thermal, dynamical, and star formation equilibrium are all satisfied.

We note that for a given Σ and $f_{\rm diff}$, which fixes $\Sigma_{\rm GBC}$ and therefore $\Sigma_{\rm SFR}$, G_0' and $P_{\rm two\text{-}phase}$ for the cooling curve, the ISM conditions would still be consistent with a two-phase medium for all values of the midplane pressure $P_{\rm th}$ between $P_{\rm min,cold}$ and $P_{\rm max,warm}$. Since $P_{\rm th}$ varies approximately $\propto (\tilde{f}_w/\alpha)^{1/2} = \tilde{f}_w(\tilde{f}_w + v_t^2/c_w^2)^{-1/2}$ (see Equation (12)), even with $\tilde{f}_w \to 1$ the midplane pressure would increase by less than a factor of 2 (remaining $< P_{\rm max,warm}$) compared to the solution assuming $\tilde{f}_w = 0.5$. A value $\tilde{f}_w \sim 0.2$ would reduce $P_{\rm th}$ by a factor ~ 2 to approach $P_{\rm min,cold}$.

Although a range of $\tilde{f}_w$ is thermodynamically permitted, self-consistent numerical simulations are required to ascertain how wide a range of $\tilde{f}_w$ can actually be realized, since a number of physical processes enter in setting $\tilde{f}_w$. For a given $f_{\rm diff}$ and Σ and hence a given heating rate (and thus a fixed thermal equilibrium curve), solutions with a larger fraction of the diffuse mass in the cold phase have lower total energy; thermal instability and condensation of warm gas into cold clouds thus tends to drive the system toward lower $\tilde{f}_w$. This is limited, however, by turbulent mixing and thermal conduction, which tend to raise $\tilde{f}_w$ and also produce out-of-equilibrium gas (see, e.g., Piontek & Ostriker 2005, 2007; Audit & Hennebelle 2005). Another consideration is that if the value of $\tilde{f}_w$ is too large (or too small), GBCs would not form sufficiently rapidly (or would form too rapidly) to maintain an equilibrium population with a total surface density $\Sigma_{\rm GBC} = (1 - f_{\rm diff})\Sigma$. Yet another issue is that the turbulent

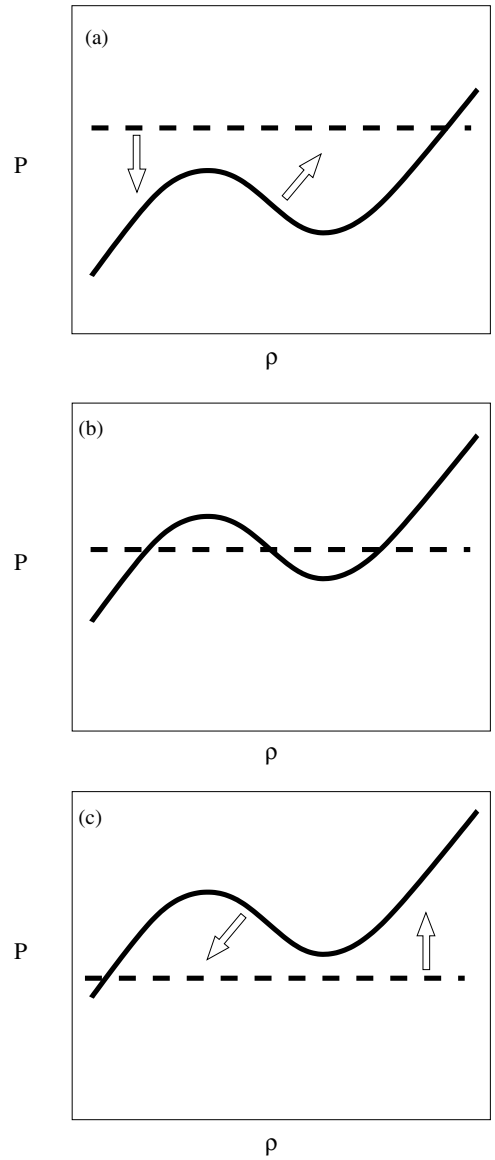

Figure 1. Schematic of approach to overall equilibrium. In (a), a higher-than-equilibrium value of the diffuse fraction $f_{\rm diff}$ makes the midplane pressure in the diffuse gas (dashed line) too high, while weak heating when the bound-cloud abundance $1 - f_{\rm diff}$ is lower-than-equilibrium makes the thermal equilibrium curve (solid line) lie at too-low pressure. In (c), $f_{\rm diff}$ is lower-than-equilibrium, making the midplane pressure in the diffuse gas (dashed line) too low; at the same time, excess heating due to a high abundance of star-forming bound clouds situates the thermal equilibrium curve (solid line) too high. In (b), $f_{\rm diff}$ is appropriate for simultaneous dynamical and thermal equilibrium with $P_{\rm th}$ at the midplane equal to $P_{\rm two\text{-}phase}$. Arrows in (a) and (c) indicate the direction of evolution of the midplane pressure level and thermal equilibrium curve for $f_{\rm diff}$ to approach the equilibrium value.

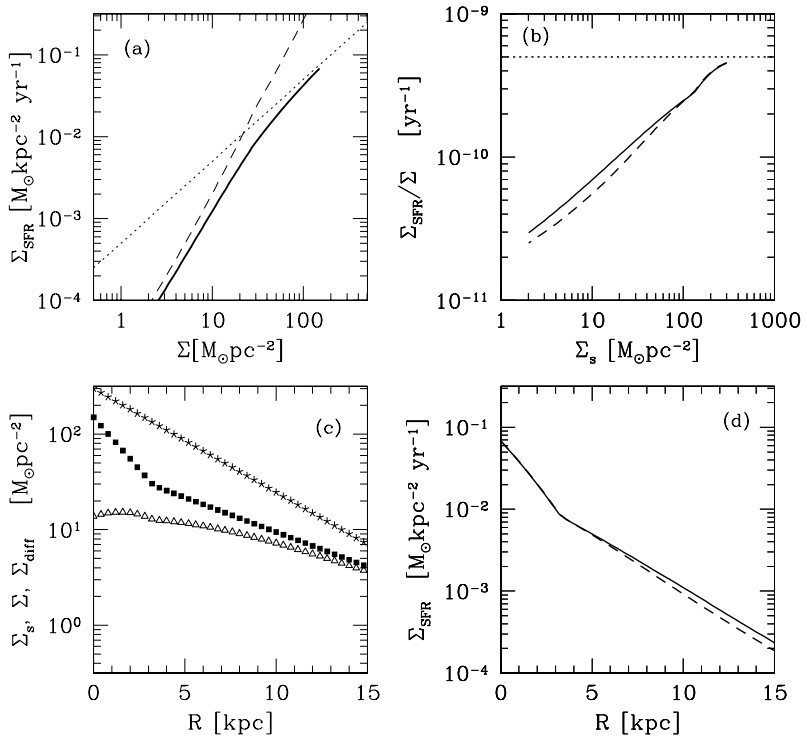

Figure 2. Sample solution of the self-consistent star formation rate for an idealized galactic model: (a) Σ_{SFR} as a function of Σ (solid), together with the maximum possible rate Σ/t_{SF} (dotted), and the outer-disk limiting solution given in Equation (22) (dashed); (b) the ratio Σ_{SFR}/Σ as a function of Σ_s, together with the maximum value $1/t_{SF}$ (dotted); (c) the input stellar surface density Σ_s (stars) and input total gas surface density Σ (squares) as a function of radius, together with the solution for Σ_{diff} (triangles), all as a function of galactic radius R; (d) the solution for Σ_{SFR} as a function of R. In (b) and (d), in addition to the case of constant stellar disk thickness (solid), results for a flaring disk $H_s \propto 1/\Sigma_s$ are shown as dashed lines.

velocity dispersion v_t in the diffuse gas is likely maintained largely by energy inputs from star formation; with a lower star formation rate and v_t, the value of $\tilde{f}_w$ would also have to decrease in order to maintain vertical dynamical equilibrium. With self-consistent numerical simulations, it will be possible to assess whether $\tilde{f}_w$ and $P_{th}/P_{two\text{-}phase}$ secularly depend on Σ and ρ_{sd}. For present purposes, we proceed under the (observationally motivated) assumptions that $P_{th} \approx P_{two\text{-}phase}$ and $\tilde{f}_w \sim 0.5$–1. The former assumption is also motivated by theory, as discussed in Section 2.4.

2.7. Sample Solution for an Idealized Galaxy

As an example of the predictions from this model, we consider an idealized disk galaxy in which the stellar surface density obeys an exponential, $\Sigma_s(R) = \Sigma_s(0)\exp(-R/R_s)$; the total gaseous surface density obeys a two part exponential, $\Sigma(R) = \Sigma_{g1}(0)\exp(-R/R_{g1})$ for the inner disk, and similarly for the outer disk with Σ_{g2} and R_{g2}; and the rotation velocity contribution from the dark matter halo is $V(R) = V_c[1-\exp(-R/R_h)]$. Setting model parameters equal to $\Sigma_s = 300\,M_\odot$ pc^{-2}, $\Sigma_{g1} = 150\,M_\odot$ pc^{-2}, $\Sigma_{g2} = 50\,M_\odot$ pc^{-2}, $R_s = 4$ kpc, $R_{g1} = 2$ kpc, $R_{g2} = 6$ kpc, $V_c = 200$ km s^{-1}, and $R_h = 1$ kpc, Figure 2 shows the adopted surface density profiles as well as the solution for Σ_{SFR} and Σ_{diff}.

For this example, results shown in Figures 2(a) and (c) adopt a constant stellar disk thickness H_s such that $\rho_s = \Sigma_s/(0.54R_s)$ following Leroy et al. (2008).[9] The solution is not very sensitive to this choice, however; to show this, in Figures 2(b) and (d), we compare results for both constant-thickness stellar disk $H_s = \text{const} \equiv H_{S,0}$ and flaring stellar disk $H_s(R) = H_{S,0}\Sigma_s(R_s)/\Sigma_s(R)$. In general, from Equation (22), $\Sigma_{SFR}/\Sigma \propto \rho_{sd}^{1/2}$ in the outer disk. Thus, if the stellar disk dominates, $\Sigma_{SFR}/\Sigma \propto \rho_s^{1/2} \propto (\Sigma_s/H_s)^{1/2}$, which yields either $\Sigma_{SFR}/\Sigma \propto \Sigma_s^{1/2}$ if H_s =const, or $\Sigma_{SFR}/\Sigma \propto \Sigma_s$ if the outer disk is flaring with $v_{z,s}$ = const and $H_s = v_{z,s}^2/(\pi G\Sigma_s)$. If the dark matter density dominates the stellar density in the outer disk, then since $\rho_{dm} \propto (V_c/R)^2$, constant V_c would imply $\Sigma_{SFR}/\Sigma \propto R^{-1}$ in the outer disk.

The example shown illustrates several characteristic features that are in accord with the recent observational results of Bigiel et al. (2008) and Leroy et al. (2008). First, it is evident that star formation does not have a sharp cutoff in the outer disk, but instead the rate gradually declines with R and Σ_s (see also the *Galaxy Evolution Explorer* (*GALEX*) observations of Boissier et al. 2007). Second, there are two regimes evident for Σ_{SFR} and Σ_{diff} versus Σ: a high-surface-density regime in which the gas is mostly in self-gravitating clouds and the limiting solution $\Sigma_{SFR} = \Sigma/t_{SF}$ is approached, and a low-surface-density regime in which Σ_{SFR} has a steeper dependence. From Equation (22), the predicted limiting behavior in outer disks (or dwarfs) is $\Sigma_{SFR} \propto \Sigma\rho_{sd}^{1/2}$, so that a dropoff in the stellar and dark matter density with R steeper than we have adopted, or a decline in Σ with R shallower than we have adopted (for a given $\rho_{sd}(R)$), would yield a steeper dependence of Σ_{SFR} on Σ in the outer disk.[10] That is, there is no single universal slope predicted for the Schmidt law in outer disks, since $\rho_{sd}^{1/2}$ need not obey a power law

[9] Note that this choice of coefficient may underestimate the midplane density somewhat. For the local Milky Way, which has $\rho_s = 0.04\,M_\odot$ pc^{-3} (Holmberg & Flynn 2000) and $\Sigma_s = 42\,M_\odot$ pc^{-2} (Holmberg & Flynn 2004) from dynamical mass models, a scale length of $R_s = 2.6$ kpc (Jurić et al. 2008) would yield $\Sigma_s/(0.54R_s) = 0.03\,M_\odot$ pc^{-3}.

[10] Note that in the limit of Σ constant, the Schmidt-law slope would be infinite, because each value of $\rho_{sd}(R)$ would yield a different value of Σ_{SFR}.

$\propto \Sigma^p$. In individual galaxies, observations in fact show a range of behaviors for $\Sigma_{\rm SFR}$ versus Σ ranging from steep declines to slow taper at low Σ, with an upper envelope $\Sigma_{\rm SFR} = \Sigma/t_{\rm SF}$ at high Σ.

An interesting feature evident in Figure 2 is that, even while the total gas surface density rises sharply in the inner disk, $\Sigma_{\rm diff}$ does not. It is straightforward to set an upper limit on $\Sigma_{\rm diff}$: from Equation (9), $\Sigma_{\rm diff} < \alpha P_{\rm th}/(\pi G \Sigma_{\rm GBC})$; using $\Sigma_{\rm GBC} = \Sigma_{\rm SFR} t_{\rm SF}$ and Equation (18),

$$\Sigma_{\rm diff} < 36\, M_\odot\ {\rm pc}^{-2} \frac{\alpha}{1 + 3\left(\frac{Z'_d \Sigma}{\Sigma_0}\right)^{0.4}}. \quad (24)$$

The physical reason for this limit is that in regions of very active star formation, the enhancement in UV heating—which tends to produce diffuse atomic gas—coincides with stronger compression of the gas by the gravity of the massive, star-forming clouds. Under high-pressure conditions, the cooling rate increases; if the diffuse-gas density is too high, cooling will exceed heating, and diffuse gas will be driven into the self-gravitating component. Since $\alpha \sim 2$–10 (see Equation (8)) with a value ~3–5 most likely, the formal limit in Equation (24) starts to become constraining only in inner galaxies where $\Sigma/\Sigma_0 \gg 1$. As discussed in the Appendix (see Equation (A22)), in fact the terms from the (variable) stellar and dark matter gravity in Equation (9) reduce $\Sigma_{\rm diff}$ by another factor ~ 2 relative to the upper limit in Equation (24).

In adopting $G'_0 = \Sigma_{\rm SFR}/\Sigma_{\rm SFR,0}$ for Equation (15), we have neglected optical depth effects. In regions of high $\Sigma_{\rm diff}$ and/or high Z' such that the optical depth is high, the mean (scaled) UV intensity G'_0 within the diffuse gas is reduced (by a factor $\sim [1 - E_2(\tau_\perp/2)]/\tau_\perp$; this varies $\propto 1/\tau_\perp$ for large $\tau_\perp$), consequently lowering $P_{\rm th}$ and, via Equation (9), $\Sigma_{\rm diff}$ itself. Thus, the current simple theory overestimates $\Sigma_{\rm diff}$ in the central parts of galaxies, where $\tau_\perp$ becomes large. We further note (see Section 4) that the value of $\Sigma_{\rm diff}$ is not equivalent to the surface density of atomic gas, since GBCs can have atomic envelopes (or even be mostly atomic at low Z) and since diffuse gas can be molecular (at high ΣZ).

2.8. Additional Considerations

Finally, we remark on a few additional points related to assumptions behind and application of the theory presented above.

(1) *Correction for hot gas.* The formulae we have developed assume that on the scales over which horizontal averages are taken, the area filling factor of hot gas $f_{\rm hot}$ is negligible. In comparing to observations, if the fraction of the area in a beam that is primarily warm+cold gas is $1 - f_{\rm hot}$, then the true surface density of warm+cold gas, for the purpose of computing dynamical and thermal equilibrium, is $\Sigma = \Sigma_{\rm obs}/(1 - f_{\rm hot})$, and similarly for $\Sigma_{\rm diff}$ and $\Sigma_{\rm GBC}$. For given $\Sigma_{\rm obs}$, increasing $f_{\rm hot}$ would tend to increase the gaseous gravity terms in Equation (11) relative to the stellar/dark matter term, and would raise the overall value of the midplane pressure.

(2) *The parameter* $\tilde{f}_w$. In the foregoing analysis, we have treated $\tilde{f}_w$ as an exogenous parameter that—based on observations—does not vary strongly within a given galaxy or from one galaxy to another. In reality, the relative proportions of cold and warm atomic gas must be self-consistently determined by considering the overall cycle of gas among phases, a highly complex problem. By considering a simple limiting case, however, it is possible to see why $\tilde{f}_w$ might have only moderate variation. We suppose that the primary way GBCs form is through self-gravitating collection of the cold diffuse atomic medium, at a rate per unit area $\Sigma_c/t_{g,c}$ where $t_{g,c} \sim (G\Sigma_c/(\sqrt{2\pi}\, H_c))^{-1/2}$ is the self-gravitational timescale for the distribution of cold atomic clouds, which has total surface density $\Sigma_c \approx (1 - \tilde{f}_w)\Sigma_{\rm diff}$ and vertical thickness $H_c \sim v_t/\sqrt{4\pi G \rho_{\rm sd}}$ (in the case where stars and dark matter dominate the vertical gravity). We also suppose that GBCs have mean lifetimes $t_{\rm GBC}$ (~ 20 Myr; e.g., Blitz et al. 2007), such that the rate of destruction of the gravitationally bound component per unit area is $\Sigma_{\rm GBC}/t_{\rm GBC} = \Sigma_{\rm SFR} t_{\rm SF}/t_{\rm GBC}$. Equating the formation and destruction rates yields

$$1 - \tilde{f}_w = \left(\frac{t_{\rm SF}}{t_{\rm GBC}}\right)^{2/3} \left(\frac{v_t^2}{2G^3}\right)^{1/6} \frac{\Sigma_{\rm SFR}^{2/3}}{\Sigma_{\rm diff} \rho_{\rm sd}^{1/6}}. \quad (25)$$

Substituting in solar-neighborhood parameters on the right-hand side, this yields $\tilde{f}_w \sim 0.6$, in agreement with local observed estimates. Next, if we consider the diffuse-dominated $\Sigma_{\rm diff} \approx \Sigma$ limit of Equation (22) (applicability of this limit includes the solar neighborhood) and substitute in $\Sigma_{\rm SFR} \propto \Sigma\sqrt{\tilde{f}_w \rho_{\rm sd}}$ on the right-hand side of Equation (25), we see that $(1 - \tilde{f}_w)/\tilde{f}_w^{1/3} \propto (\rho_{\rm sd}/\Sigma^2)^{1/6}$. The weak dependence on both $\rho_{\rm sd}$ and Σ^2, and the fact that only their ratio appears so that variations will be partially compensated, implies that $\tilde{f}_w$ would indeed be expected to vary only modestly, at least in outer disks.

Of course, the above is an (oversimplified) description of only one of the possible ways in which GBCs might form. Understanding how $\tilde{f}_w$ depends on the fundamental environmental properties of a galaxy (Σ, $\rho_{\rm sd}$, metallicity) will require numerical simulations that follow a wide range of processes, including realistic treatment of turbulence (which can alter $\tilde{f}_w$ via small-scale local mixing, and can also collect diffuse gas into GBCs if large-scale flows with long durations are present).

(3) *Galactic and metagalactic radiation.* In adopting $G'_0 = \Sigma_{\rm SFR}/\Sigma_{\rm SFR,0}$, we have assumed that the contribution from metagalactic UV is small compared to the locally generated intensity (and neglected the slowly varying dependence on optical depth). Sternberg et al. (2002) estimate that the ratio of metagalactic to locally generated UV in the solar neighborhood is 0.0024. The star formation rate could therefore decline to ~ 0.002 times the local value, or $6 \times 10^{-6}\, M_\odot\ {\rm kpc}^{-2}\ {\rm yr}^{-1}$, before the metagalactic UV becomes important; this occurs only in the far-outer regions of disks. In this regime, instead of using $G'_0 = \Sigma_{\rm SFR}/\Sigma_{\rm SFR,0}$ in Equation (15), a constant value ~ 0.002 would be substituted. Beyond this point, $P_{\rm two\text{-}phase}$ would be essentially constant from Equation (15), and the midplane pressure (given by Equation (21)) would fall below $P_{\rm min,cold}$ (as in Figure 1(c)). Beyond this point, the diffuse gas would be essentially all warm, and star formation could only occur to the extent that gas is externally compressed, e.g., by spiral density waves. In practice, since in our theory $\Sigma_{\rm SFR} \propto \Sigma\sqrt{\rho_{\rm sd}} \propto \Sigma V_c/R$ in outer disks if dark matter dominates the gravity, the gas may reach sufficiently low surface density ($\sim 0.1\, M_\odot\ {\rm pc}^{-2}$; see Sternberg et al. 2002) that it could be ionized by metagalactic X-rays before the point where $\Sigma \lesssim 0.002\, M_\odot\ {\rm pc}^{-2} R/{\rm kpc}$ is reached. In addition to true metagalactic radiation, the contribution to the UV intensity originating nonlocally within a galaxy climbs as the local optical depth drops. At very low optical depths where $J_{\rm FUV} \propto \Sigma_{\rm SFR} \ln(1/\tau_\perp)$, the star formation rate would be reduced below that in Equation (22) by a factor $\sim 1/\ln(1/\tau_\perp)$; this varies $\propto 1/R$ if the gas surface density

obeys an exponential. In far outer galaxy regions, the radiation from the inner galaxy may exceed that produced by local star formation, especially if the disk is strongly flaring.

(4) *Properties of GBCs.* In this work, we have not focused on the details of individual GBCs, beyond making the simplifying assumption that the gas in these structures forms stars on a timescale $t_{\rm SF}$ that does not significantly vary from one cloud to another. At a fundamental level (see McKee & Ostriker 2007), the star formation timescale within a GBC is expected to depend on the mean density (which sets the mean gravitational free-fall time $t_{\rm ff}$) and on the amplitude of turbulence and strength of the magnetic field (since these properties determine how gas is further compressed and rarefied).

If the star formation rate in a GBC is defined to be $\varepsilon_{\rm ff} M_{\rm cloud}/t_{\rm ff}$, then $t_{\rm SF,GBC} = t_{\rm ff}/\varepsilon_{\rm ff}$, where $t_{\rm ff} = (\pi M_{\rm cloud}/\Sigma_{\rm cloud}^3)^{1/4}(8G)^{-1/2}$ in terms of the cloud's mass and mean surface density. Krumholz & McKee (2005) have argued that, due to the lognormal form of the density distribution in turbulent clouds, $\varepsilon_{\rm ff}$ will depend only weakly on a cloud's internal turbulent Mach number, which itself varies as $v_{\rm turb}/v_{\rm th} \propto (M_{\rm cloud}\Sigma_{\rm cloud})^{1/4} T_{\rm cloud}^{-1/2}$. As a consequence, $t_{\rm SF,GBC}$ is not expected to vary very strongly with a cloud's properties; e.g., Krumholz & McKee (2005) propose a scaling which yields $t_{\rm SF,GBC} \propto M_{\rm cloud}^{1/3}\Sigma_{\rm cloud}^{-2/3} T_{\rm cloud}^{-1/6}$. As noted above, GBCs are composed of both molecular (shielded) and atomic (shielding) gas. Because the atomic gas has temperature somewhat higher ($\lesssim 100$ K) than that of the molecular gas ($\lesssim 10$ K), the star formation efficiency may vary within a given GBC, as well as varying from one cloud to another. Since the temperature is determined by cooling, it depends on whether carbon is mostly atomic or in CO, with the latter holding in the more-shielded parts of clouds (Wolfire et al. 2010). In a more refined theory, these intra- and intercloud variations could be taken into account in determining a mean value of $t_{\rm SF,GBC}$ (for an assumed cloud mass function); here, we have simply adopted a single constant value, $t_{\rm SF}$.

It is worth emphasizing again that the GBC component in our model is not equivalent to the molecular component observed in galaxies. An individual GBC is composed of a mixture of molecular gas and cold atomic gas that depends on shielding, and could be primarily atomic at sufficiently low metallicity. For spherical clouds, $(M_{\rm atom}/M_{\rm mol})_{\rm cloud} \approx [Z'^{0.8}(N_{\rm H,cloud}/1.8\times10^{21}\ {\rm cm^{-2}}) - 0.7]^{-1}$ (Krumholz et al. 2009a; McKee & Krumholz 2010). Although the chemistry of GBCs depends strongly on Z, the temperature of the cold gas is relatively insensitive to metallicity at high density $n_H \gtrsim 100\,{\rm cm^{-3}}$ (e.g., Wolfire et al. 1995). Thus, the internal dynamics of primarily atomic GBCs—including the processes that determine the internal star formation efficiency—are expected to be similar to those in primarily molecular GBCs, provided that their gravitational potentials and internal velocity dispersions are similar so that $v_{\rm turb} \gg v_{\rm th,cold}$.

We note that Krumholz et al. (2009b) have developed a model for galactic star formation rates under an alternative set of assumptions. In their model, interstellar gas is assumed to be gathered into complexes with mean surface densities $\Sigma_{\rm complex} \sim 5\Sigma$, where Σ is averaged over $\sim$ kiloparsec scales. The fraction of mass within complexes that participates in star formation is determined by shielding. The molecular gas is assumed to be in GMCs with a surface density equal to the value observed in local galaxies, $\Sigma_{\rm cloud} = 85\,M_\odot\ {\rm pc^{-2}}$, provided this exceeds the mean gas surface density. Stars form in the GMCs at a rate determined by the Krumholz & McKee (2005) theory. In this model, $\Sigma_{\rm SFR}$ becomes a steep function of Σ when complexes become primarily atomic, for ISM surface density $\Sigma \lesssim (20/Z')(\Sigma/\Sigma_{\rm complex})\,M_\odot\ {\rm pc^{-2}}$. The Krumholz et al. (2009b) model makes fewer assumptions and extends to higher-Σ conditions than the model discussed here. However, while it is successful in describing the average properties of star-forming galaxies, it is substantially less accurate than the present model in describing the star formation in individual galaxies, which is discussed below.

3. COMPARISON TO OBSERVATIONS

The formulae derived above yield predictions for $\Sigma_{\rm SFR}$ as a function of galactic gas and stellar properties, and can be compared with observations. Here, we compare with a recent survey of spiral galaxies, for which the gas, stellar, and star formation content is described in detail in Leroy et al. (2008). The observed measurements include molecular and atomic gaseous surface densities, $\Sigma_{\rm mol}$ and $\Sigma_{\rm atom}$ (based on CO $J = 2$–1 and 1–0 maps and on H I 21 cm maps, respectively, and corrected for helium), rotation curves $V_c(R)$, stellar surface densities Σ_s (based on 3.6 μm *Spitzer* maps), and star formation surface densities $\Sigma_{\rm SFR}$ (based on FUV maps from *GALEX* and 24 μm *Spitzer* maps). The surveyed regions include both molecule-dominated and atomic-dominated areas, extending to $\sim 1.2 r_{25}$.

Here, we estimate stellar densities in two ways, taking the disk scale height $H_s = $ const so that $\rho_s(R) = \Sigma_s(R)/(0.54R_s)$ following Leroy et al. (2008); and taking $H_s \propto 1/\Sigma_s$ (i.e., a flared disk) so that $\rho_s(R) = \Sigma_s^2(R)/[0.54R_s\Sigma_s(R_s)]$, where R_s is the fitted exponential scale length of the stellar disk. We estimate dark matter densities using observed rotation curves, as $\rho_{\rm dm}(R) = (V_c^2 - V_{c,s}^2)/(4\pi G R^2)$, where $V_{c,s}^2/R$ is the correction for the contribution to the radial acceleration from the stellar disk (this correction is $\lesssim$50% in the outer disk, where the contribution to vertical gravity from dark matter becomes significant). Given ρ_s, $\rho_{\rm dm}$, and total gas surface density $\Sigma = \Sigma_{\rm atom} + \Sigma_{\rm mol}$ at each radius R, we numerically solve the equations developed in Section 2 to obtain predictions for $\Sigma_{\rm diff}$ and $\Sigma_{\rm SFR}$ (see the Appendix for details). For the initial comparisons presented here, we use annular averages of the data sets in each galaxy; "pointwise" comparisons we have made at map resolutions of 800 pc show similar results, in terms of the mean values and the scatter in the observations and model predictions.

For the galaxy NGC 7331, Figures 3 and 4 present results for model predictions compared to the observations, for flat and flared stellar disk cases $H_s = $ const and $H_s \propto 1/\Sigma_s$, respectively. For this galaxy, we have used the fitted metallicity profile of Dutil & Roy (1999) and assumed $Z'_d = Z'_g$, for Equation (18). We have adopted the fiducial values $\alpha = 5$ and $\tilde{f}_w = 0.5$ for the diffuse-ISM parameters, as discussed in Section 2. The values of $\Sigma_{\rm SFR}$ and $\Sigma_{\rm SFR}/\Sigma$ are shown as functions of R, Σ, and Σ_s. Also shown are the input profiles of Σ_s, $\Sigma = \Sigma_{\rm atom} + \Sigma_{\rm mol}$, and $\Sigma_{\rm atom}$, together with the predicted $\Sigma_{\rm diff}$. Evidently, the model provides a remarkably good prediction for $\Sigma_{\rm SFR}$, with a slightly better match for the flared-disk case ($\lesssim$ 20% differences) than for the flat-disk case ($\lesssim$ 50% differences). In particular, the prediction follows the observation quite well in the atomic-dominated regime (see Figure 4), outside of $\approx$7 kpc. We note that with slight adjustments of $\tilde{f}_w/\alpha$, the flaring of the stellar disk, or the dark matter density compared to the standard parameters and prescriptions, even closer agreement between predicted and observed $\Sigma_{\rm SFR}$ can be obtained. Figures 3 and 4 show that the model result for $\Sigma_{\rm diff}$ exceeds $\Sigma_{\rm H\,I}$ in the inner region of the galaxy. While some of the diffuse gas in

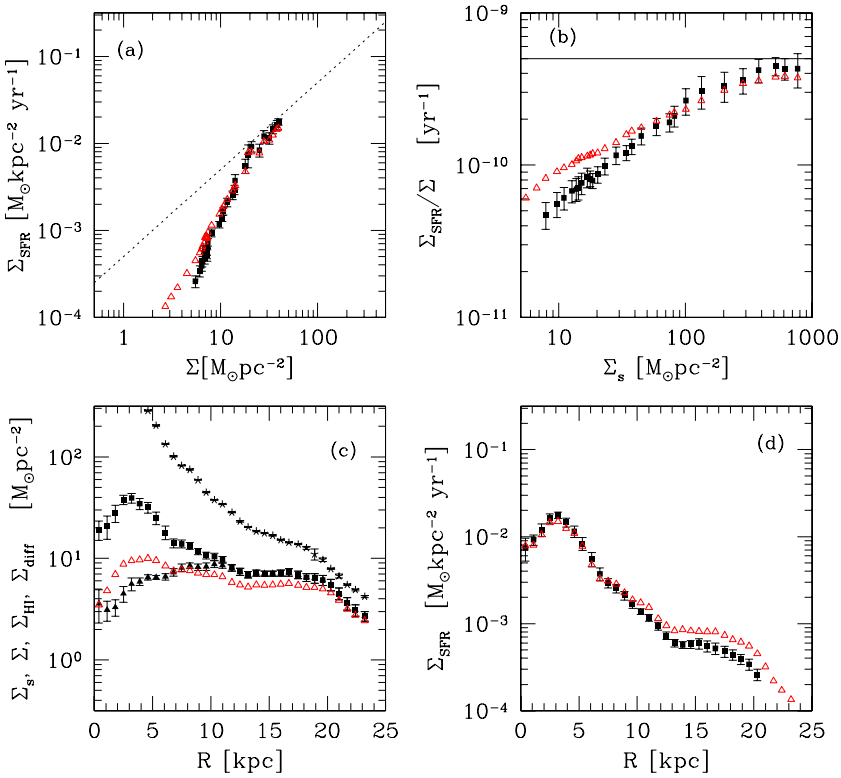

Figure 3. Comparison between observed annular averages and model prediction for the galaxy NGC 7331. In (a), (b), and (d), filled squares with error bars show the observed values of Σ_{SFR} or Σ_{SFR}/Σ, where Σ is the total gas surface density; open triangles (red) show the predictions from the theory of Section 2. In (c), stars show the observed stellar surface density Σ_s, squares show total observed Σ, filled triangles show the observed atomic gas surface density, and open triangles (red) show the model prediction for the diffuse-gas surface density Σ_{diff}. For the observations, error bars indicate scatter in the values within each azimuthal ring (systematic errors are larger). For the model prediction, H_s = const is adopted for the stellar scale height.

(A color version of this figure is available in the online journal.)

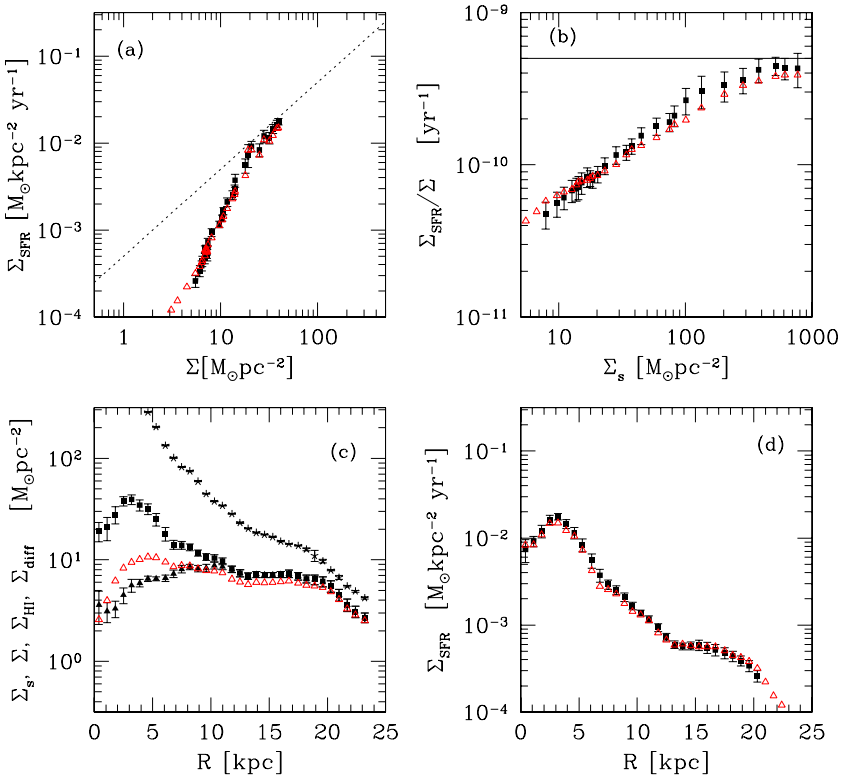

Figure 4. Same as in Figure 3, except a flaring stellar disk with $H_s \propto 1/\Sigma_s$ is adopted.

(A color version of this figure is available in the online journal.)

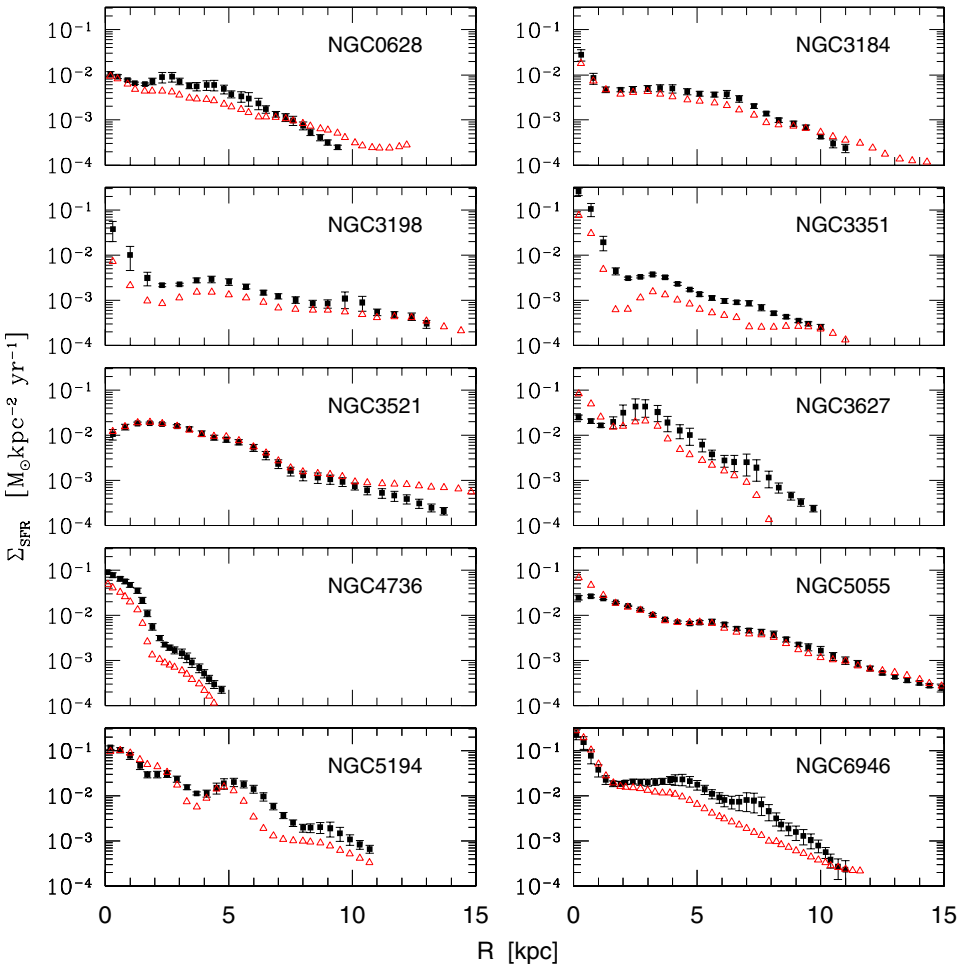

Figure 5. Comparison between observed annular averages of Σ_{SFR} (black squares) and model prediction (red triangles), for a set of spiral galaxies. For the model, H_s = const is adopted.

(A color version of this figure is available in the online journal.)

galactic center regions could in fact be molecular, we note (see Section 2.7) that our neglect of radiative transfer in estimating J_{FUV} makes Σ_{diff} increasingly inaccurate in regions of high Σ. This does not affect the predicted value of Σ_{SFR}, however, because $\Sigma_{diff} \ll \Sigma$.

For the remaining set of 10 spiral galaxies in the sample, Figures 5 and 6 show the comparison between observed and predicted values of Σ_{SFR}, for H_s = const and $H_s \propto 1/\Sigma_s$. As for NGC 7331, we adopt the fiducial parameter values $\tilde{f}_w = 0.5$ and $\alpha = 5$; no corrections for departures from the solar gas-to-dust ratio have been made, however. Overall, the predictions follow the observed profiles fairly well. For NGC 5055, which, like NGC 7331, is a flocculent galaxy, quite good agreement is evident ($\lesssim 30\%$ differences for H_s = const or $\lesssim 50\%$ differences for $H_s \propto 1/\Sigma_s$). Again, this is true both for the inner molecule-dominated region, and for the atomic-dominated region which lies outside of ≈ 8 kpc. When considering azimuthally averaged data, it is not surprising that the prediction should be most accurate for flocculent galaxies: since the dependence of Σ_{SFR} on Σ is nonlinear at high Σ, the prediction for the average Σ_{SFR} using the azimuthally averaged Σ can significantly underestimate the average using local values of Σ if the gas and star formation are both strongly concentrated in spiral arms (see Equation (A20) in the Appendix). Note that both NGC 7331 and NGC 5055 are also observed to have particularly clean linear relationships between Σ_{SFR} and Σ_{mol}.

For a few cases (e.g., NGC 3198, NGC 4736, NGC 5194), the shape of the predicted Σ_{SFR} follows that of the observations in the atomic-dominated part, but with an offset downward in the overall magnitude. From Equation (22), $\Sigma_{SFR} \propto (\tilde{f}_w/\alpha)^{1/2}$ in the diffuse-gas-dominated regime, so that adopting a number for $\tilde{f}_w/\alpha$ larger than the fiducial value we have assumed would shift the predicted Σ_{SFR} upward. Of course, it is also possible that observational systematics contribute to this offset. For NGC 4736, the inner molecular-dominated regime has an offset between predicted and observed $\log(\Sigma_{SFR})$ that is similar to the outer-disk offset. Since the predicted Σ_{SFR} in inner disks is $\propto t_{SF}^{-1}$ but independent of $\tilde{f}_w$ and α, the similarity of the inner- and outer-disk offsets could either mean that t_{SF}^{-1} and $(\tilde{f}_w/\alpha)^{1/2}$ happen to vary together, or that the observed star formation rate is systematically overestimated everywhere (note that this galaxy has other peculiarities in both its star formation and gas dynamics; see Wong & Blitz 2000). The galaxies NGC 3198 and 3351 have observed values of Σ/Σ_{SFR} in their inner regions less than the fiducial value $t_{SF} = 2 \times 10^9$ yr; potentially, the gas surface density may be underestimated if the CO-to-H_2 conversion factor is too small, or star formation rates may be overestimated.

For some other galaxies (e.g., NGC 0628, NGC 6946, and to a lesser extent, NGC 3184), the shape of the predicted and observed Σ_{SFR} differ somewhat. The sense of the discrepancy

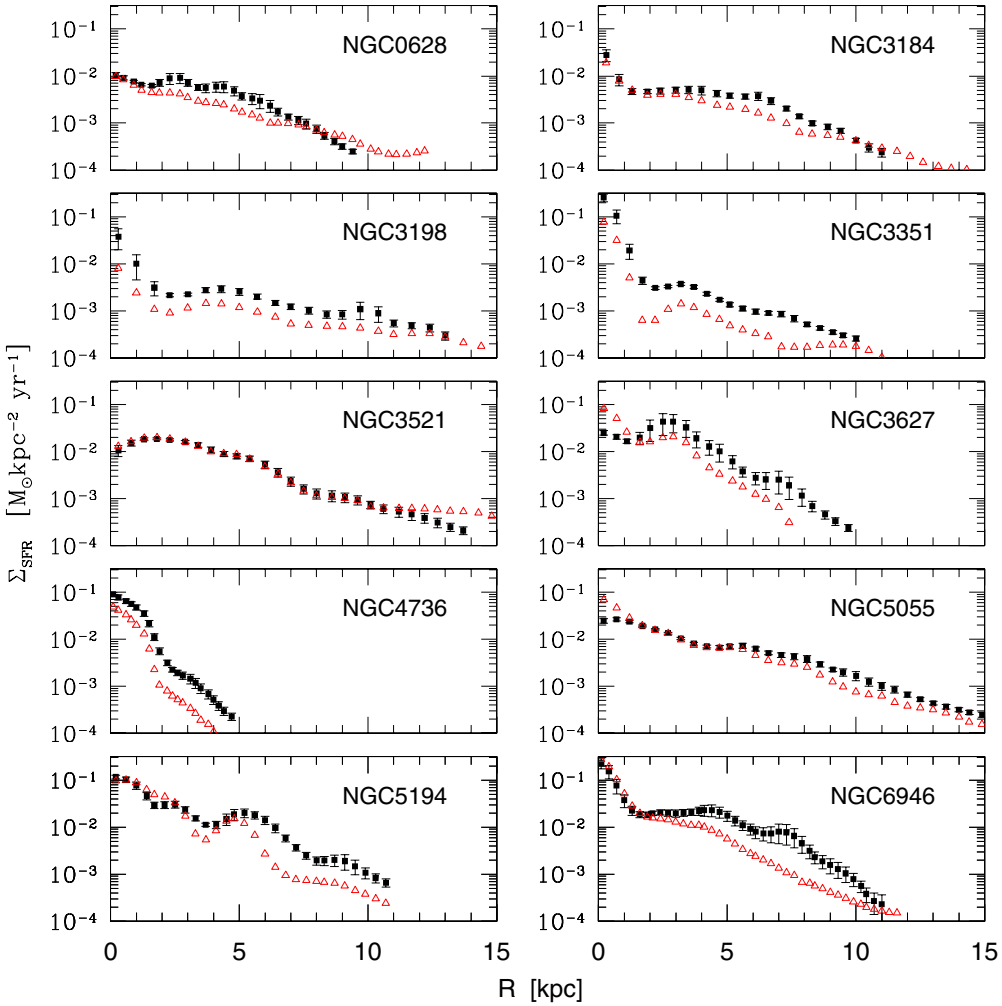

Figure 6. Same as in Figure 5, except $H_s \propto 1/\Sigma_s$ is adopted for the model.
(A color version of this figure is available in the online journal.)

is that the observed Σ_{SFR} is higher than the predicted value at intermediate radii. If some star-forming gas is present that is not observable either in 21 cm or CO lines, this could in part account for the discrepancy. These galaxies also have an irregular— and sublinear on average—relationship between Σ_{SFR} and Σ_{mol} as inferred from CO. This might indicate that CO is not a linear tracer of the gas in GBCs, that $t_{SF,GBC}$ is not constant in these regions, or that age effects in the stellar population are impacting the estimate of Σ_{SFR}.

Blitz & Rosolowsky (2006) obtained an empirical fit relating the molecular-to-atomic-gas mass fractions to a midplane pressure estimate, $\Sigma_{mol}/\Sigma_{atom} = (P_h/P_{h,0})^\gamma$, for

$$P_h = P_{BR} \equiv \Sigma(2G\rho_s)^{1/2} v_g. \quad (26)$$

This pressure estimate assumes that the stellar disk dominates the vertical gravity, and combines the atomic and molecular gas into a single component. When combined with $\Sigma_{SFR} = \Sigma_{mol}/t_{SF}$, this yields

$$\Sigma_{SFR} = \frac{\Sigma}{t_{SF}} \frac{(P_h/P_{h,0})^\gamma}{1 + (P_h/P_{h,0})^\gamma}. \quad (27)$$

Blitz & Rosolowsky (2006) adopted a vertical velocity dispersion $v_g = 8$ km s^{-1}, and obtained values $\gamma = 0.92$ and $P_{h,0}/k \approx 4 \times 10^4$ cm^{-3} K for the fitting constants.

Leroy et al. (2008) found that a similar relationship fits their sample of spirals, with $\gamma = 0.8$, $P_{h,0}/k = 1.7 \times 10^4$ cm^{-3} K, and a pressure estimate that includes gas self-gravity:

$$P_h = P_L \equiv \frac{\pi G \Sigma^2}{2} + \Sigma(2G\rho_s)^{1/2} v_g; \quad (28)$$

the adopted value for the vertical velocity dispersion of the composite ISM is $v_g = 11$ km s^{-1}. Note that the gravity of dark matter is not included in either the Blitz & Rosolowsky (2006) or the Leroy et al. (2008) pressure estimate; dark matter may be increasingly important in far outer disks or in low-surface-brightness disks.

For $P_h/P_{h,0} \gg 1$, Equation (27) yields the same star formation rate as that in the GBC-dominated regime for the present model, $\Sigma_{SFR} \rightarrow \Sigma/t_{SF}$. For $P_h/P_{h,0} \ll 1$, the limit in which atomic gas dominates molecular gas, Equation (27) yields $\Sigma_{SFR} \rightarrow \Sigma(P_h/P_{h,0})^\gamma/t_{SF}$. Since γ is close to unity for both of these empirical relations, and Σ in the diffuse-dominated limit for both samples is typically ~ 5–$10\, M_\odot$ pc^{-2} so that P_h varies approximately as $\rho_s^{1/2}$, these relationships are similar to the form of our result given in Equation (22) (see also Equation (A13)). (Note that a value of γ less than 1 partially compensates for varying Σ in P_h.) As an example, Figure 7 presents the comparison between our model results and the

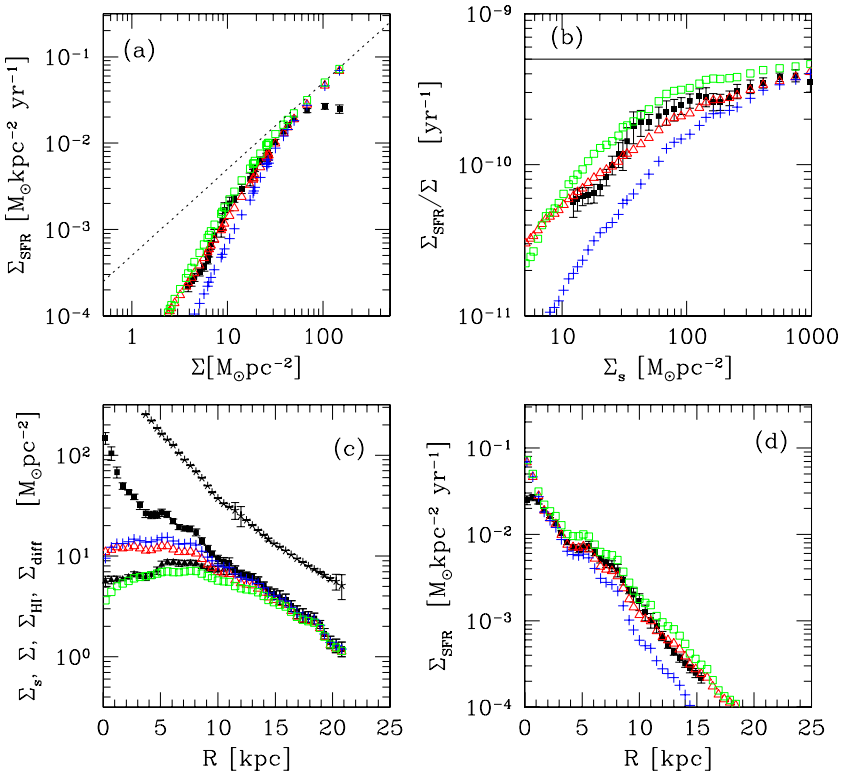

Figure 7. Same as in Figure 3, for the galaxy NGC 5055. Also included is the comparison with the empirical formulae of Blitz & Rosolowsky (2006; blue plusses) and Leroy et al. (2008; green boxes), as described in the text.

(A color version of this figure is available in the online journal.)

empirical fits given above, for the galaxy NGC 5055. For this and other galaxies, we find a close correspondence particularly with the empirical formula of Leroy et al. (2008; as discussed above, slightly larger $\tilde{f}_w/\alpha$ than our fiducial choice shifts our predicted Σ_{SFR} upward). The empirical formula of Blitz & Rosolowsky (2006) produces somewhat more rapid decline in Σ_{SFR} at low Σ (for large radii) than the prediction of our model.

4. SUMMARY AND DISCUSSION

(1) *Summary of the physical model.* In this paper, we have developed a theory for self-regulated star formation in multiphase galactic ISM disks in which stellar heating mediates the feedback. The fundamental principles we adopt are that for a time-and-space-averaged steady state on $\sim$ kiloparsec scales, (a) force balance must be satisfied in the vertical direction, dynamically setting the midplane thermal pressure P_{th} of the diffuse gas based on the weight of overlying material (see Equation (11)); (b) thermal equilibrium must be satisfied, with the heating rate set by the local star formation rate (see Equations (15) and (16)), and with the two-phase thermal equilibrium pressure $P_{two\text{-}phase}$ in the diffuse gas equal to the dynamically imposed equilibrium pressure P_{th}; and (c) the star formation rate is controlled by the amount of gas in GBCs (see Equation (19)), with the (complementary) non-self-gravitating amount regulated by the thermal pressure (see Equation (9)).

The set of algebraic equations embodying the principles above can easily be solved numerically to obtain Σ_{SFR} as a function of the total gas surface density Σ and the midplane stellar-plus-dark-matter density ρ_{sd}, as described in the Appendix. An approximate closed-form solution, representing the key result of this work, is given by Equations (22) and (23). In the diffuse-gas-dominated regime, $\Sigma_{SFR} \propto \Sigma\sqrt{\rho_{sd}}$ (see Equation (22)). As a consequence, no single Schmidt-type relation $\Sigma_{SFR} \propto \Sigma^{1+p}$ is expected to apply in outer disks, since $\sqrt{\rho_{sd}}$ need not vary as Σ^p.

Physically, outer and inner disks are distinguished by which gas component dominates the mass—diffuse or self-gravitating. Where diffuse gas dominates, the mean pressure and density and hence the cooling rate are fixed by the weight of the ISM. The amount of self-gravitating, star-forming gas created is then tuned to provide the needed FUV heating to balance cooling at this density: $\Sigma_{SFR} \propto P_{th} \propto \Sigma\sqrt{\rho_{sd}}$. Where self-gravitating gas dominates so that $\Sigma_{SFR} \propto \Sigma$, the specific heating rate is fixed. The cooling rate of the diffuse gas depends on its density, which is proportional to the surface density Σ_{diff} (and to the vertical gravity); Σ_{diff} must therefore adjust until the cooling rate matches the heating rate. The limited surface density observed for H I gas in the central regions of galaxies likely owes at least in part to the constraint imposed by matching heating with cooling in the diffuse ISM.

(2) *Connection to previous work.* Our theory makes use of some of the same concepts—such as thermal and dynamic equilibrium—discussed in previous work, but with a different emphasis. Parravano (1988) suggested that star formation is self-regulated in such a way that the UV radiation it produces maintains $P_{max,warm}$ near the thermal pressure of the gas, and Parravano & Mantilla (1991) applied this model to the Milky Way by adopting a radial profile for the warm gas density. Considering outer galaxies, Elmegreen & Parravano (1994) pointed out that star formation could be strongly suppressed in outer disks if the midplane pressure falls sufficiently far below $P_{min,cold}$ that even locally compressed regions cannot cool. Schaye (2004), treating the UV intensity as a fixed parameter,

suggested that star formation would have a threshold imposed by thermodynamics. Here, we propose that (low-level) star formation is able to extend out to large radii in galactic disks because $P_{\rm min,cold}$ adjusts to follow the outward decline in the midplane pressure, via a decrease in the UV flux (tracking the decline in the star formation rate).

In our model, star formation is regulated such that UV radiation created by young stars heats the disk just as much as is needed for the thermal pressure in the diffuse gas to meet the requirements imposed by vertical force balance. The regulation process depends on mass exchange between self-gravitating and diffuse components of the ISM such that star formation at the required rate can take place in the bound clouds. Since the star formation rate in normal galaxies is proportional to the mass in gravitationally bound GMCs, we believe that this self-regulation mechanism is the physical basis for the relationship between molecular surface density and midplane pressure empirically identified by Blitz & Rosolowsky (2004, 2006). The theoretical relationship we obtain is in fact slightly different from the empirical formula of Blitz & Rosolowsky (2006; see also Leroy et al. 2008). They found that the ratio of molecular-to-atomic surface densities is approximately proportional to an estimate of the total midplane pressure for a composite ISM (see Section 3 for details), whereas here we argue that the surface density of gas contained in GBCs should be proportional to the midplane thermal pressure in the diffuse gas. While physically and mathematically different, the two relationships yield quantitatively similar values of $\Sigma_{\rm SFR}$ provided the atomic surface density is relatively uniform (as is true in the observations of Blitz & Rosolowsky 2004, 2006 and Leroy et al. 2008), the ratio of thermal to total pressure is relatively constant, and the gas in GBCs is mostly molecular. In particular, the empirical BR relationship is most sensitive in the atomic-dominated limit, where the predicted star formation rate (assuming constant-$t_{\rm SF}$ in molecular gas) is similar in form to our theoretical outer-disk law, $\Sigma_{\rm SFR} \propto \Sigma\sqrt{\rho_{\rm sd}}$.

(3) *Comparison to observation, present and future.* Initial comparisons of predicted star formation rates with observed values, based on azimuthally averaged data for disk galaxies, show quite promising results. In particular, the predictions follow the observations very closely throughout the two large flocculent galaxies NGC 7331 and NGC 5055, out to $1.2r_{25}$. In these initial comparisons, we have not "tuned" the model parameters α, $\tilde{f}_w$, or $t_{\rm SF}$ at all, but simply adopted the same values for all the galaxies in the sample. By adjusting the parameters, closer agreement between the model prediction and observations can be obtained in several cases, by shifting the overall normalization of $\Sigma_{\rm SFR}$. Adjusting the prescription for converting stellar surface density to volume density can also yield a closer match to the data.

Current data sets exist that make it possible to extend the present comparisons in several ways, including using $\sim$ kiloparsec resolution maps (also including local variations of the gas-to-dust ratio) rather than azimuthally averaged data, and considering dwarf galaxies. For far outer disks, the necessary averaging scale is likely to increase, due to the flaring of the disk. It will be interesting to test whether galaxies with strong spiral structure, when examined locally, are consistent with the steady-state theory developed here, or whether transient effects within spiral arms are too rapid for (quasi-)equilibrium to be attained.

In the analysis of Section 2, we employ several parameters (e.g., $\tilde{f}_w$, α, $t_{\rm SF}$, and the ratio of solar-neighborhood pressure to star formation rate), adopting fiducial values that are based on current observations and/or theoretical work. As more detailed ISM information becomes available from extragalactic observations (such as local values of the gaseous vertical velocity dispersion, and the proportions of atomic gas in warm and cold phases), it will be possible to assign observed values rather than adopted parameters as inputs for predicting $\Sigma_{\rm SFR}$ within individual galaxies. With local measurements of the stellar vertical velocity dispersion in the outer parts of individual face-on galaxies, it will be possible to obtain more direct estimates of the stellar midplane density, rather than simply adopting a prescription for the stellar scale height to obtain ρ_s from Σ_s. From surveys of edge-on galaxies, it will also be possible to obtain accurate measurements of the correlations of stellar disk flaring with other properties, that could then be applied to more face-on systems statistically. With more detailed data sets, it will be possible to test constituent elements of the theory—including Equations (7) and (18)—as well as the overall prediction for $\Sigma_{\rm SFR}$.

(4) *Opportunities for numerical modeling.* It is of considerable interest to test the idealizations of this theory, as well as its predictions, via detailed numerical simulations. Numerical models must have sufficiently fine spatial grids ($\lesssim$ pc) that the vertical direction is well resolved, must include heating and cooling such that warm and cold phases are present, and must model energetic feedback (leading to both heating and turbulent driving) from star formation in self-gravitating clouds. Because turbulent mixing at extremely small scales ($\ll$ parsecs) can affect $\tilde{f}_w$, it is important to assess this effect using very high resolution simulations (e.g., Audit & Hennebelle 2005).

With simulations, the turbulent velocity dispersion and warm/cold fractions in the diffuse medium can be self-consistently calculated (cf. Koyama & Ostriker 2009a), such that the dependence of the ISM "state" parameters α and $\tilde{f}_w$ on the (input) galactic environment "variables" (Σ, ρ_s, $\rho_{\rm dm}$, Z) and (derived) star formation rate $\Sigma_{\rm SFR}$ can be assessed. The star formation timescale $t_{\rm SF}$ in GBCs and the ratio of mean thermal pressure (or mean FUV intensity) to $\Sigma_{\rm SFR}$ are also in principle calculable theoretically, although the dependence on the fundamental environment variables may be fairly complex.

While we have not discussed here exactly how the formation of GBCs takes place, this can in principle be strongly affected by the angular momentum of the disk, with disks having very low or high Toomre Q departing from observed star formation and molecular/atomic (or GBC/diffuse) relations at a given Σ and ρ_s (Koyama & Ostriker 2009a, 2009b). Normal galaxies have had sufficient time to evolve (lowering Σ and raising ρ_s by converting gas into stars) that the fundamental dependence of $\Sigma_{\rm SFR}$ on angular momentum and shear may, however, not be evident in practice. Thus, exploring a wide range of types of observed systems, and testing both realistic and unrealistic galaxy models with numerical simulations, will be important for revealing the processes that control star formation at the most fundamental level.

(5) *Limitations and prospects.* By adopting a fixed value of the star formation timescale $t_{\rm SF}$ in self-gravitating clouds, the present model is limited to the regime in which star-forming clouds have "normal" properties, similar to those observed in the disks of Local Group galaxies (e.g., Sheth et al. 2008; Bolatto et al. 2008). In particular, it is not applicable to galactic center regions or starbursts where Σ exceeds the typical surface density $\sim 100\,M_\odot$ pc^2 of individual mid-disk GMCs. In such high-Σ regions, molecular gas completely dominates the ISM,

but because the average density is higher than in mid-disk GMCs—so that the gravitational time $\propto \rho^{-1/2}$ is shorter, the star formation rate per unit mass is expected to be higher than it is for "normal" GMCs (consistent with observations). In detail, the star formation rate per unit mass in bound clouds in high-Σ regions is also expected to depend on the turbulence level (which is higher in starbursts) and whether star-forming clouds are collapsing or marginally bound (cf. Krumholz & McKee 2005; Rosas-Guevara et al. 2010; Padoan & Nordlund 2009). Thus, from a combination of these effects, $\Sigma_{\rm SFR}/\Sigma_{\rm GBC}$ is not expected to be constant in high-Σ regions, and the present theory should not be applied there.

We note that low-metallicity systems, where GBCs are less self-shielded and have larger atomic-to-molecular ratios than "normal" GMCs of the same size and mass, may also have values of $\Sigma_{\rm SFR}/\Sigma_{\rm GBC}$ different from the constant value $t_{\rm SF}^{-1} = (2\times10^9)^{-1}$ yr we have adopted (based on the CO observations of Bigiel et al. 2008). In bound clouds with a large atomic-gas proportion (and with the carbon mostly atomic rather than in CO), the mean temperature will be larger than that in primarily molecular clouds. Because of the lower internal Mach number, turbulent compression would be less extreme than in colder, primarily molecular, clouds, which could affect the fraction of gas that is able to collapse and make stars. Additional observational and theoretical work is needed to evaluate how the star-forming efficiencies of bound clouds depend on relative amounts of cold atomic versus molecular gas, and also to explore whether the masses and/or total column densities of star-forming bound clouds in low-metallicity regions (far-outer disks of spirals, and dwarf galaxies) differ systematically from the properties of "normal" GMCs. Observationally, a difficulty (particularly in low-metallicity regions) is that significant gas can be "dark" (Grenier et al. 2005)—i.e., not observable either in H I (because the hydrogen is molecular) or in CO (because the carbon is atomic). For solar metallicity and clouds with $A_V \sim 8$, the fraction of "dark" gas is expected to be only ~ 0.3 (Wolfire et al. 2010).

The present model does not address radiative transfer effects explicitly. In particular, we have assumed that the optical depth through the diffuse gas is modest, such that the mean UV intensity and therefore the thermal pressure is approximately proportional to the local $\Sigma_{\rm SFR}$ (see Equations (15)–(18)). Although this approximation becomes invalid where $\Sigma_{\rm diff} \gtrsim 20/Z'\,M_\odot$ pc^{-2} (for Z' the metallicity relative to solar), typically $\Sigma \gg \Sigma_{\rm diff}$ by this point (see, e.g., Figure 2), so that changes in the FUV intensity and hence $P_{\rm two\text{-}phase}$ and $P_{\rm th}$ would not significantly affect the predicted $\Sigma_{\rm SFR}$. An accurate determination of $\Sigma_{\rm diff}$ where $\Sigma Z'$ is high would, however, require an explicit radiative transfer calculation to assess G_0' for a given value of $\Sigma_{\rm SFR}$. This would be affected both by the amount and vertical distribution of diffuse gas, and by radiative transfer within star-forming clouds themselves. Radiative transfer effects also become important in the far-outer regions of galaxies, where heating from nonlocal UV can exceed the local contribution. Results of radiative transfer models could in principle be tested by comparison to multiwavelength IR observations, since the dust temperature is sensitive to G_0' (i.e., to the mean UV intensity $J_{\rm FUV}$) (Draine et al. 2007). Here, we have not attempted to address these issues, but instead we have simply adopted an empirical solar-neighborhood value for the ratio of $J_{\rm FUV}$ to $\Sigma_{\rm SFR}$ to calibrate our relationships.

Determination of the relative proportions of atomic and molecular (and, for low Σ, ionized) gas also depends on radiative transfer. For GBCs, the solution for spherical clouds of Krumholz et al. (2009a) and McKee & Krumholz (2010) predicts the molecular-to-atomic ratio is $(M_{\rm atom}/M_{\rm mol})_{\rm cloud} \approx [Z'^{0.8}(N_{\rm H,cloud}/1.8\times10^{21}\,{\rm cm}^{-2}) - 0.7]^{-1}$; if clouds either have fixed total hydrogen column density or there is a known relationship between the mean surface density of this gas component $\Sigma_{\rm GBC}$ (averaged over $\sim$ kpc scales) and the column density of individual clouds, then this could be used to compute the contributions to $\Sigma_{\rm mol}$ and $\Sigma_{\rm atom}$ from $\Sigma_{\rm GBC}$. The diffuse gas could also be partly molecular; using the results of McKee & Krumholz (2010) for a slab of cold gas illuminated on both sides, a layer begins to become molecular when $\Sigma_{\rm cold} \gtrsim 11\,M_\odot$ pc$^{-2}/[Z'^{0.8}]$.

Finally, we note that simple models of the kind we have developed here—if validated by detailed numerical simulations and confirmed by observations—potentially provide a valuable tool for studies of galaxy evolution. We caution, however, that careful appraisal of metallicity effects will be required before applying this model (or a refined version) to star formation in galaxies at high redshift. Our results could also potentially be adapted to provide subgrid ISM/star formation prescriptions for use in cosmological simulations of galaxy formation, but this too should be approached with care since the ratio of diffuse to gravitationally bound gas is computed not for a local three-dimensional zone but for a vertically integrated disk. Even with a subgrid model, the scale height of the diffuse warm+cold ISM ($H \sim \sigma_z^2/g_z \sim \sigma_z/\sqrt{4\pi G\rho_{\rm tot}}$) must be resolved by several zones in order to obtain an accurate estimate for the midplane pressure, which controls the amount of star-forming gas. Because formation of gravitationally bound star-forming clouds depends on nonlocal dynamical processes, simulations that are either resolved sufficiently to capture gravitationally induced vertical motions, or are completely vertically unresolved with a suitable prescription for balance of ISM components, can represent the relevant physics more faithfully than simulations which resolve the disk with just a few zones.

The work of E.C.O. was supported in part by fellowships from the Miller Institute at U.C. Berkeley and the John Simon Guggenheim Foundation, and by grants AST-0908185 from the National Science Foundation and NNG05GG43G from NASA. The work of C.F.M. was supported in part by grant AST-0908553 from the National Science Foundation. C.F.M. also acknowledges the support of the Groupement d'Intérêt Scientifique (GIS) "Physique des deux infinis (P2I)." Support for A.K.L. was provided by NASA through Hubble Fellowship grant HST-HF-51258.01-A awarded by the Space Telescope Science Institute, which is operated by the Association of Universities for Research in Astronomy, Inc., for NASA, under contract NAS 5-26555. We are grateful to Bruce Elmegreen, Rob Kennicutt, and Antonio Parravano for helpful comments on the manuscript, and to the referee for a thoughtful and constructive report.

APPENDIX

Here, we provide an explicit formula that is solved numerically to obtain the fractions of diffuse and gravitationally bound gas. We show how this formula leads to the Equations (22) and (23) given in the text for the star formation rate. We also discuss how the galactic environment variables (Σ, $\rho_{\rm sd}$, Z) and the ISM model parameters control the transition between the diffuse-dominated and GBC-dominated regimes, and how presence of both regimes in a given annulus (due to spiral structure)

affects estimates of the star formation rate. Finally, we provide a more stringent upper limit on $\Sigma_{\rm diff}$ than the limit given by Equation (24) in the text.

We start with the diffuse-gas thermal equilibrium Equation (18) relating the thermal pressure to the star formation rate $\Sigma_{\rm SFR} = \Sigma_{\rm GBC}/t_{\rm SF}$, which may be expressed as

$$P_{\rm th} = \frac{1}{\phi_d}\frac{P_{\rm th,0}}{\Sigma_{\rm SFR,0}}\frac{\Sigma_{\rm GBC}}{t_{\rm SF}}. \tag{A1}$$

Here, $P_{\rm th,0}$ and $\Sigma_{\rm SFR,0}$ are the solar-neighborhood thermal pressure of diffuse gas and star formation rate that we adopt for our normalizations, and

$$\phi_d \equiv \frac{1}{4}\left[1 + 3\left(\frac{Z'_d\Sigma}{\Sigma_0}\right)^{0.4}\right] \tag{A2}$$

is defined such that it is equal to unity for $\Sigma = \Sigma_0$, the solar-neighborhood diffuse-gas surface density. The ratio of $P_{\rm th,0}$ to the mean local FUV intensity $J_{\rm FUV,0}$ is computed theoretically (Wolfire et al. 2003), so that solar-neighborhood observations effectively enter the model through the ratio $J_{\rm FUV,0}/\Sigma_{\rm SFR,0}$. Using solar-neighborhood values $P_{\rm th,0}/k = 3000\ {\rm K\,cm^{-3}}$ and $\Sigma_{\rm SFR,0} = 2.5\times10^{-9}\,M_\odot\ {\rm pc^{-2}\ yr^{-1}}$ with $t_{\rm SF} = 2\times10^9$ yr as determined from extragalactic studies, this yields $P_{\rm th}/k = 600\ {\rm K\,cm^{-3}}\phi_d^{-1}(\Sigma_{\rm GBC}/\,M_\odot\ {\rm pc^{-2}})$ for the relation between thermal pressure and the surface density of gas in GBCs (star-forming).[11]

Next, we define

$$\Sigma_{\rm diff} \equiv x\Sigma, \tag{A3}$$

$$\Sigma_{\rm GBC} \equiv (1-x)\Sigma, \tag{A4}$$

for the diffuse-gas and GBC surface densities, substituting these expressions together with Equation (A1) for $P_{\rm th}$ in Equation (9) to obtain

$$x\Sigma = \{\pi G\Sigma_h\Sigma(1-x)\}\{\pi G\Sigma(1-x) + [(\pi G\Sigma)^2(1-x)^2 + (\pi G)^2\Sigma\Sigma_h(1-x) + 8\pi G\zeta_d c_w^2\tilde{f}_w\alpha\rho_{\rm sd}]^{1/2}\}^{-1}. \tag{A5}$$

Here, we have introduced

$$\Sigma_h \equiv \frac{2\alpha P_{\rm th,0}}{\pi G\phi_d\Sigma_{\rm SFR,0}t_{\rm SF}} = 91\,M_\odot\ {\rm pc^{-2}}\phi_d^{-1}\left(\frac{\alpha}{5}\right)\left(\frac{P_{\rm th,0}/k}{3000\ {\rm K\,cm^{-3}}}\right) \times\left(\frac{\Sigma_{\rm SFR,0}}{2.5\times10^{-9}\,M_\odot\ {\rm pc^{-2}\ yr^{-1}}}\right)^{-1}\left(\frac{t_{\rm SF}}{2\times10^9\ {\rm yr}}\right)^{-1}. \tag{A6}$$

Since $P_{\rm th,0}/(\phi_d\Sigma_{\rm SFR,0}t_{\rm SF}) = P_{\rm th}/\Sigma_{\rm GBC}$ and $\alpha P_{\rm th}$ is the total (effective) midplane pressure, Σ_h is the value that Σ would have to attain in order for the total pressure to equal $\pi G\Sigma\Sigma_{\rm GBC}/2$; that is, for the pressure to be dominated by the gravity of the gas.

Next, we define

$$S \equiv \frac{8\zeta_d\alpha\tilde{f}_w c_w^2}{\pi G}\frac{\rho_{\rm sd}}{\Sigma^2} \tag{A7}$$

$$= 31\left(\frac{\alpha}{5}\right)\left(\frac{\tilde{f}_w}{0.5}\right)\left(\frac{\rho_{\rm sd}}{0.1\,M_\odot\ {\rm pc^{-3}}}\right)\left(\frac{\Sigma}{10\,M_\odot\ {\rm pc^{-2}}}\right)^{-2}, \tag{A8}$$

which measures the relative importance of external gravity (stellar-disk+dark matter) to gas self-gravity in setting the diffuse-gas pressure. We note that if $\rho_{\rm sd}$ is dominated by stars with $\rho_s = \Sigma_s/(2H_s) = \pi G\Sigma_s^2/(2v_{z,s}^2)$,

$$S = 4\zeta_d\frac{\langle v_{\rm th}^2 + v_t^2\rangle}{v_{z,s}^2}\frac{\Sigma_s^2}{\Sigma^2}, \tag{A9}$$

which is $\propto (Q_{\rm gas}/Q_s)^2$ in terms of the stellar and gas Toomre parameters (cf. Equation (4) in Koyama & Ostriker 2009b). Using fiducial values $\alpha = 5$ and $\tilde{f}_w = 0.5$, $S \sim 16$ in the solar neighborhood.

We can now re-express Equation (A5) in terms of the dimensionless variables S and

$$w \equiv \frac{\Sigma}{\Sigma_h}, \tag{A10}$$

yielding

$$\frac{1}{x} = w\left\{1 + \left[1 + \frac{1}{(1-x)w} + \frac{S}{(1-x)^2}\right]^{1/2}\right\}. \tag{A11}$$

Given values of $\rho_{\rm sd}$ and Σ in a galaxy, the variables S and w are set, and we can solve the (cubic) Equation (A11) for x numerically. The root x is bounded by 0 and 1, so we use the bisection method. Given a solution for the diffuse-gas fraction x, the star formation rate is then

$$\Sigma_{\rm SFR} = (1-x)\frac{\Sigma}{t_{\rm SF}}. \tag{A12}$$

We use this numerical solution to obtain the star formation rates for both our idealized galaxy (Figure 2), and for the comparison of the model prediction to the observed star formation rates (Figures 3–7).

One important limit is that in which the ISM is dominated by diffuse gas, in which case $x \to 1$, and Equation (A11) yields

$$1 - x \to w\frac{1 + [1+4S]^{1/2}}{2} \approx w(1 + S^{1/2}). \tag{A13}$$

When multiplied by Σ and divided by $t_{\rm SF}$, this yields Equation (22) of the text.

Equation (A13) requires $w(1+S^{1/2}) \ll 1$ for self-consistency, whereas $x \to 0$ in Equation (A11) requires $w(1+S^{1/2}) \gg 1$. An approximate solution for $1-x$ allowing for both limits is

$$\frac{1}{1-x} \approx \frac{1}{w(1+S^{1/2})} + 1. \tag{A14}$$

The inverse of this, when multiplied by Σ and divided by $t_{\rm SF}$, yields the approximation for the star formation rate given by

[11] Note that inserting $\Sigma_{\rm GBC} \lesssim 2\,M_\odot\ {\rm pc^{-2}}$, as indicated by solar-neighborhood observations of molecular gas (Dame et al. 1987, 2001; Bronfman et al. 1988; Luna et al. 2006; Nakanishi & Sofue 2006), would yield a pressure a factor of ~ 2 below the observed local value. This simply reflects the fact that $\Sigma_{\rm SFR,0} \lesssim 10^{-9}\,M_\odot\ {\rm pc^{-2}\ yr^{-1}}$ if $\Sigma_{\rm GBC} \lesssim 2\,M_\odot\ {\rm pc^{-2}}$ and $t_{\rm SF} = 2\times10^9$ yr, whereas observational estimates of $\Sigma_{\rm SFR,0}$ are higher by a factor ~ 2 (Bertelli & Nasi 2001; Vergely et al. 2002; Fuchs et al. 2009). It is uncertain whether this discrepancy is the result of an underestimate of the local $\Sigma_{\rm GBC}$, an overestimate of the local $\Sigma_{\rm SFR}$, or a lower local value for $t_{\rm SF}$ than the mean extragalactic value.

Equation (23) of the text. Since $w \lesssim 1$ for the regions we are considering in this paper, it is generally the value of $wS^{1/2}$ (which depends on $\rho_{\rm sd}$ but not on Σ) that determines which star formation regime holds. The approximation for $1-x$ given in Equation (A14) is good to within 11% for $S \geqslant 10$ and $w \geqslant 0.01$; for $w \leqslant 0.2$ and $0.1 \leqslant S \leqslant 10$, a better approximation (good to within 12%) is obtained by using $0.5[1+(1+4S)^{1/2}]$ instead of $1+S^{1/2}$ (cf. Equation (A13)).

Using Equation (A14) and the definitions of w and S, the overall timescale for gas to be converted to stars is given by

$$t_{\rm con} \equiv \frac{\Sigma}{\Sigma_{\rm SFR}} = \frac{t_{\rm SF}}{1-x} \tag{A15}$$

$$\approx \frac{P_{\rm th,0}}{\phi_d \Sigma_{\rm SFR,0}} \left(\frac{\alpha}{2\pi G \zeta_d c_w^2 \tilde{f}_w \rho_{\rm sd}} \right)^{1/2} + t_{\rm SF}, \tag{A16}$$

where $S \gg 1$ is assumed for the latter expression. This timescale will be set by whichever of the two terms is larger. The first term is proportional to the vertical oscillation time, $\sqrt{\pi/(G\rho_{\rm sd})}$, which controls how fast cold cloudlets can sink to the midplane and form GBCs (for our fiducial parameter choices, this term in $t_{\rm con}$ is 39 times the vertical oscillation time). The second term is the characteristic time for gas within GBCs to form stars.

Quantitatively, the transition between the diffuse-dominated and GBC-dominated cases occurs where $x = 1/2$. From Equation (A11), this yields the condition

$$w_{1/2} = \frac{2}{3}(1 - Sw^2) = \frac{2}{3}\left(1 - \frac{8\zeta_d \alpha \tilde{f}_w c_w^2 \rho_{\rm sd}}{\pi G \Sigma_h^2}\right), \tag{A17}$$

where Σ_h is given in Equation (A6). Since the right-hand side depends only $\rho_{\rm sd}$, this gives a value for the transition surface density $\Sigma_{1/2} = w_{1/2}\Sigma_h$ as a function of $\rho_{\rm sd}$. Taking the fiducial parameter choices, $Sw^2 = 0.37(\rho_{\rm sd}/0.1\,M_\odot\ {\rm pc}^{-3})$. For a given value of $\rho_{\rm sd}$, the ISM will be diffuse dominated if $\Sigma < \Sigma_{1/2}$, and GBC dominated if $\Sigma > \Sigma_{1/2}$. For example, at the solar circle where $\rho_{\rm sd} = 0.05\,M_\odot\ {\rm pc}^{-3}$, the transition from diffuse dominated to GBC dominated would occur at $\Sigma_{1/2} = 0.54\Sigma_h \sim 50\,M_\odot\ {\rm pc}^{-2}$. We note that if $\rho_{\rm sd}$ is large enough that $Sw^2 > 1$, then $x < 1/2$ (i.e., $\Sigma_{\rm GBC} > \Sigma_{\rm diff}$) regardless of the value of Σ.

At a given galactocentric radius, if the surface density satisfies either $\Sigma \ll \Sigma_{1/2}$ or $\Sigma \gg \Sigma_{1/2}$ at all azimuthal angles, then a single star formation regime applies, and the azimuthally averaged star formation rate can be obtained from the azimuthally averaged gas surface density. If, however, there is a transition from $\Sigma < \Sigma_{1/2}$ in interarm regions to $\Sigma > \Sigma_{1/2}$ in spiral arm regions, then the star formation regime changes from diffuse dominated to GBC dominated, and the prediction of $\Sigma_{\rm SFR}$ based on $\langle\Sigma\rangle$ would depart from the true value due to nonlinearities. Equation (A14), when multiplied by $t_{\rm SF}$ and evaluated using the value of w in the arm gives $t_{\rm con,arm} \equiv \Sigma_{\rm arm}/\Sigma_{\rm SFR,arm}$ in the arm gas:

$$t_{\rm con,arm} \approx \frac{t_{\rm SF}}{w_{\rm arm} + w_{\rm arm} S_{\rm arm}^{1/2}} + t_{\rm SF} \tag{A18}$$

(note that $S \gg 1$ does *not* hold in arms, so that Equation (A16) should not be used; $w_{\rm arm}$ may however be $\gtrsim 1$). An analogous expression holds for $t_{\rm con,ia} \equiv \Sigma_{\rm ia}/\Sigma_{\rm SFR,ia}$ in the interarm region using $w_{\rm arm} \to w_{\rm ia}$ and $S_{\rm arm} \to S_{\rm ia}$. Letting $f_{\rm arm}$ be the mass fraction in the arm in a given annulus, the star formation rate in the annulus using the arm and interarm conditions separately is

$$\Sigma_{\rm SFR,arm+ia} = \frac{\langle\Sigma\rangle}{t_{\rm con,ia}}\left[1 + f_{\rm arm}\left(\frac{t_{\rm con,ia}}{t_{\rm con,arm}} - 1\right)\right]. \tag{A19}$$

At a given radius, $wS^{1/2} \propto \rho_{\rm sd}^{1/2}$ varies by $\lesssim 10\%$ from spiral perturbations, so that $w_{\rm ia}S_{\rm ia}^{1/2} \approx w_{\rm arm}S_{\rm arm}^{1/2} \to wS^{1/2}$. For most regions of interest, $w_{\rm ia} \ll wS^{1/2} \ll 1$ so that $t_{\rm con,ia} \approx t_{\rm SF}(wS^{1/2})^{-1}$. Equation (A19) can be compared to the star formation rate that would be estimated using $\langle\Sigma\rangle$ in Equation (A14), which yields $\Sigma_{\rm SFR,az} = \langle\Sigma\rangle(1-x)_{\rm az}/t_{\rm SF} \approx \langle\Sigma\rangle wS^{1/2}/t_{\rm SF} \approx \langle\Sigma\rangle/t_{\rm con,ia}$ (assuming $\langle w\rangle \ll wS^{1/2}$). Taking the ratio of $\Sigma_{\rm SFR,arm+ia}$ to $\Sigma_{\rm SFR,az}$, we obtain

$$\frac{\Sigma_{\rm SFR,arm+ia}}{\Sigma_{\rm SFR,az}} \approx 1 + f_{\rm arm}\left(\frac{w_{\rm arm}}{wS^{1/2}[w_{\rm arm} + wS^{1/2} + 1]}\right). \tag{A20}$$

Since the term in parentheses is typically order unity, the true star formation rate (i.e., $\Sigma_{\rm SFR,arm+ia}$) can be considerably larger than the estimate $\Sigma_{\rm SFR,az}$ based on the annular azimuthal average $\langle\Sigma\rangle$ if the gas is highly concentrated in the arms.

Finally, we consider the upper limit on the diffuse-gas surface density. Taking the inverse of Equation (A11) and multiplying by Σ, we have for the diffuse-gas surface density

$$\Sigma_{\rm diff} = \frac{\Sigma_h}{1 + \left(1 + \frac{\Sigma_h}{\Sigma(1-x)} + \frac{S}{(1-x)^2}\right)^{1/2}} \tag{A21}$$

$$< \frac{\Sigma_h}{1 + \left(1 + \frac{\Sigma_h}{\Sigma} + S\right)^{1/2}}. \tag{A22}$$

The right-hand side of the inequality (A22) is the limiting value of $\Sigma_{\rm diff}$ for $x \ll 1$, i.e., the case in which the ISM is dominated by GBCs. An absolute upper limit $\Sigma_{\rm diff} < \Sigma_h/2$ is obtained by taking $\Sigma_h/\Sigma, S \to 0$; the result is given by Equation (24) of the text. In practice, the terms Σ_h/Σ and S in the denominator of Equation (A22) are appreciable, so that $\Sigma_{\rm diff}$ is below $\Sigma_h/2$ by a factor of a few.

REFERENCES

Abramova, O. V., & Zasov, A. V. 2008, Astron. Rep., 52, 257
Audit, E., & Hennebelle, P. 2005, A&A, 433, 1
Audit, E., & Hennebelle, P. 2010, A&A, 511, A76
Beck, R. 2008, in AIP Conf. Ser. 1085, High Energy Gamma-ray Astronomy, ed. F. A. Aharonian, W. Hofmann, & F. Rieger (Melville, NY: AIP), 83
Bertelli, G., & Nasi, E. 2001, AJ, 121, 1013
Bigiel, F., Leroy, A., Walter, F., Brinks, E., de Blok, W. J. G., Madore, B., & Thornley, M. D. 2008, AJ, 136, 2846
Blanc, G. A., Heiderman, A., Gebhardt, K., Evans, N. J., & Adams, J. 2009, ApJ, 704, 842
Blitz, L., Fukui, Y., Kawamura, A., Leroy, A., Mizuno, N., & Rosolowsky, E. 2007, Protostars and Planets V, ed. B. Reipurth, D. Jewitt, & K. Keil (Tucson, AZ: Univ. Arizona Press), 81
Blitz, L., & Rosolowsky, E. 2004, ApJ, 612, L29
Blitz, L., & Rosolowsky, E. 2006, ApJ, 650, 933
Boissier, S., Prantzos, N., Boselli, A., & Gavazzi, G. 2003, MNRAS, 346, 1215
Boissier, S., et al. 2007, ApJS, 173, 524
Bolatto, A. D., Leroy, A. K., Rosolowsky, E., Walter, F., & Blitz, L. 2008, ApJ, 686, 948
Bottema, R. 1993, A&A, 275, 16
Boulares, A., & Cox, D. P. 1990, ApJ, 365, 544
Bronfman, L., Cohen, R. S., Alvarez, H., May, J., & Thaddeus, P. 1988, ApJ, 324, 248
Dame, T. M., Hartmann, D., & Thaddeus, P. 2001, ApJ, 547, 792

Dame, T. M., et al. 1987, ApJ, 322, 706
de Blok, W. J. G., & Walter, F. 2006, AJ, 131, 363
Dickey, J. M., & Lockman, F. J. 1990, ARA&A, 28, 215
Dickey, J. M., Strasser, S., Gaensler, B. M., Haverkorn, M., Kavars, D., McClure-Griffiths, N. M., Stil, J., & Taylor, A. R. 2009, ApJ, 693, 1250
Dong, H., Calzetti, D., Regan, M., Thilker, D., Bianchi, L., Meurer, G. R., & Walter, F. 2008, AJ, 136, 479
Dopita, M. A. 1985, ApJ, 295, L5
Draine, B. T., et al. 2007, ApJ, 663, 866
Dutil, Y., & Roy, J. 1999, ApJ, 516, 62
Elmegreen, B. G. 1989, ApJ, 338, 178
Elmegreen, B. G., & Parravano, A. 1994, ApJ, 435, L121
Ferrière, K. M. 2001, Rev. Mod. Phys., 73, 1031
Fuchs, B., Jahreiß, H., & Flynn, C. 2009, AJ, 137, 266
Gaensler, B. M., Madsen, G. J., Chatterjee, S., & Mao, S. 2008, PASA, 25, 184
Gazol, A., Luis, L., & Kim, J. 2009, ApJ, 693, 656
Gazol, A., Vázquez-Semadeni, E., & Kim, J. 2005, ApJ, 630, 911
Glover, S. C. O., & Mac Low, M. 2010, arXiv:1003.1340
Goldreich, P., & Lynden-Bell, D. 1965, MNRAS, 130, 125
Grenier, I. A., Casandjian, J., & Terrier, R. 2005, Science, 307, 1292
Heiles, C., & Troland, T. H. 2003, ApJ, 586, 1067
Heiles, C., & Troland, T. H. 2005, ApJ, 624, 773
Hennebelle, P., & Audit, E. 2007, A&A, 465, 431
Heyer, M. H., Corbelli, E., Schneider, S. E., & Young, J. S. 2004, ApJ, 602, 723
Heyer, M., Krawczyk, C., Duval, J., & Jackson, J. M. 2009, ApJ, 699, 1092
Holmberg, J., & Flynn, C. 2000, MNRAS, 313, 209
Holmberg, J., & Flynn, C. 2004, MNRAS, 352, 440
Hunter, D. A., Elmegreen, B. G., & Baker, A. L. 1998, ApJ, 493, 595
Jenkins, E. B., & Tripp, T. M. 2001, ApJS, 137, 297
Jenkins, E. B., & Tripp, T. M. 2007, in IAU Symp. 237, Triggered Star Formation in a Turbulent ISM, ed. B. G. Elmegreen & J. Palous (Cambridge: Cambridge Univ. Press), 53
Joung, M. K. R., & Mac Low, M. 2006, ApJ, 653, 1266
Joung, M. R., Mac Low, M., & Bryan, G. L. 2009, ApJ, 704, 137
Jurić, M., et al. 2008, ApJ, 673, 864
Kalberla, P. M. W., & Kerp, J. 2009, ARA&A, 47, 27
Kennicutt, R. C., Jr. 1998, ApJ, 498, 541
Kennicutt, R. C., Jr., et al. 2007, ApJ, 671, 333
Kim, W.-T., & Ostriker, E. C. 2001, ApJ, 559, 70
Kim, W., & Ostriker, E. C. 2007, ApJ, 660, 1232
Komugi, S., Sofue, Y., Nakanishi, H., Onodera, S., & Egusa, F. 2005, PASJ, 57, 733
Koyama, H., & Ostriker, E. C. 2009a, ApJ, 693, 1316
Koyama, H., & Ostriker, E. C. 2009b, ApJ, 693, 1346
Krumholz, M. R., & McKee, C. F. 2005, ApJ, 630, 250
Krumholz, M. R., McKee, C. F., & Tumlinson, J. 2009a, ApJ, 693, 216
Krumholz, M. R., McKee, C. F., & Tumlinson, J. 2009b, ApJ, 699, 850
Leroy, A. K., Walter, F., Brinks, E., Bigiel, F., de Blok, W. J. G., Madore, B., & Thornley, M. D. 2008, AJ, 136, 2782
Luna, A., Bronfman, L., Carrasco, L., & May, J. 2006, ApJ, 641, 938
McKee, C. F., & Krumholz, M. R. 2010, ApJ, 709, 308
McKee, C. F., & Ostriker, E. C. 2007, ARA&A, 45, 565
Mohan, R., Dwarakanath, K. S., & Srinivasan, G. 2004, J. Astrophys. Astron., 25, 185
Nakanishi, H., & Sofue, Y. 2006, PASJ, 58, 847
Padoan, P., & Nordlund, A. 2009, arXiv:0907.0248
Parravano, A. 1988, A&A, 205, 71
Parravano, A., & Mantilla, J. C. 1991, A&A, 250, 70
Petric, A. O., & Rupen, M. P. 2007, AJ, 134, 1952
Piontek, R. A., & Ostriker, E. C. 2004, ApJ, 601, 905
Piontek, R. A., & Ostriker, E. C. 2005, ApJ, 629, 849
Piontek, R. A., & Ostriker, E. C. 2007, ApJ, 663, 183
Quirk, W. J. 1972, ApJ, 176, L9
Rosas-Guevara, Y., Vazquez-Semadeni, E., Gomez, G. C., & -Katharina Jappsen, A. 2010, MNRAS, 406, 1875
Ryder, S. D., & Dopita, M. A. 1994, ApJ, 430, 142
Salim, S., et al. 2007, ApJS, 173, 267
Schaye, J. 2004, ApJ, 609, 667
Schmidt, M. 1959, ApJ, 129, 243
Schmidt, M. 1963, ApJ, 137, 758
Schuster, K. F., Kramer, C., Hitschfeld, M., Garcia-Burillo, S., & Mookerjea, B. 2007, A&A, 461, 143
Sheth, K., Vogel, S. N., Wilson, C. D., & Dame, T. M. 2008, ApJ, 675, 330
Solomon, P. M., Rivolo, A. R., Barrett, J., & Yahil, A. 1987, ApJ, 319, 730
Sternberg, A., McKee, C. F., & Wolfire, M. G. 2002, ApJS, 143, 419
Tamburro, D., Rix, H., Leroy, A. K., Low, M., Walter, F., Kennicutt, R. C., Brinks, E., & de Blok, W. J. G. 2009, AJ, 137, 4424
Toomre, A. 1964, ApJ, 139, 1217
van der Kruit, P. C., & Searle, L. 1982, A&A, 110, 61
Vergely, J., Köppen, J., Egret, D., & Bienaymé, O. 2002, A&A, 390, 917
Verley, S., Corbelli, E., Giovanardi, C., & Hunt, L. K. 2010, A&A, 510, A64
Wolfire, M. G., Hollenbach, D., & McKee, C. F. 2010, ApJ, 716, 1191
Wolfire, M. G., Hollenbach, D., McKee, C. F., Tielens, A. G. G. M., & Bakes, E. L. O. 1995, ApJ, 443, 152
Wolfire, M. G., McKee, C. F., Hollenbach, D., & Tielens, A. G. G. M. 2003, ApJ, 587, 278
Wong, T. 2009, ApJ, 705, 650
Wong, T., & Blitz, L. 2000, ApJ, 540, 771
Wong, T., & Blitz, L. 2002, ApJ, 569, 157
Young, L. M., & Lo, K. Y. 1996, ApJ, 462, 203